Supramolecular Chemistry
Publication details, including instructions for authors and subscription information:
http://www.informaworld.com/smpp/title~content=t713649759

Differential Ion-pairing and Temperature Effects on Intervalence Charge Transfer (IVCT) in a Series of Dinuclear Ruthenium Complexes

Deanna M. D'Alessandro[a]; Peter C. Junk[b]; F. Richard Keene[a]
[a] School of Pharmacy & Molecular Sciences, James Cook University, Queensland, Australia [b] School of Chemistry, Monash University, Victoria, Australia

To cite this Article D'Alessandro, Deanna M. , Junk, Peter C. and Keene, F. Richard(2005) 'Differential Ion-pairing and Temperature Effects on Intervalence Charge Transfer (IVCT) in a Series of Dinuclear Ruthenium Complexes', Supramolecular Chemistry, 17: 7, 529 — 542
To link to this Article: DOI: 10.1080/10610270500310537
URL: http://dx.doi.org/10.1080/10610270500310537

Supramolecular Chemistry, October–November 2005 Vol. 17 (7), pp. 529–546

Differential Ion-pairing and Temperature Effects on Intervalence Charge Transfer (IVCT) in a Series of Dinuclear Ruthenium Complexes

DEANNA M. D'ALESSANDRO[a], PETER C. JUNK[b] and F. RICHARD KEENE[a,*]

[a]*School of Pharmacy & Molecular Sciences, James Cook University, Townsville, Queensland 4811, Australia;* [b]*School of Chemistry, Monash University, Clayton, Victoria 3182, Australia*

Received (in Southampton, UK) 17 June 2005; Accepted 17 August 2005

Thermochromism and anion-dependence studies on the intervalence charge transfer (IVCT) properties of the diastereoisomers of $[\{Ru(bpy)_2\}_2(\mu\text{-BL})]^{5+}$ {BL = dpb′, dpq′, and dpb: dpb′ = dipyrido(2,3-a;3′,2′-c)benzophenazine; dpq′ = dipyrido(2,3-a;3′,2′-c)phenazine; dpb = 2,3-bis(2-pyridyl)-1,4-benzoquinoxaline} are reported. IVCT thermochromism studies revealed that the level of delocalisation may differ between the diastereoisomers for a system, and a slight temperature dependence in *meso*-$[\{Ru(bpy)_2\}_2(\mu\text{-dpb})]^{5+}$ which was dependent on the identity of the counter-anion {PF_6^- or $B(C_6F_5)_4^-$} Anion effects on the IVCT properties of the diastereoisomeric forms of the three complexes were observed to be somewhat unpredictable.

X-ray crystal structure determinations on *meso*-$[\{Ru(bpy)_2\}_2(\mu\text{-dpb})]^{4+}$ (as the PF_6^- and $[ZnCl_4]^{2-}$ salts), *meso*-$[\{Ru(bpy)_2\}_2(\mu\text{-dpb}')]^{4+}$ (PF_6^- salt) and *meso*-$[\{Ru(bpy)_2\}_2(\mu\text{-dpq}')]^{4+}$($[ZnCl_4]^{2-}$ salt) revealed considerable distortion in the bridging ligand, particularly in the dpb-bridged species where the distortion was also dependent on the anion.

INTRODUCTION

An understanding of metal-metal interactions in metallosupramolecular assemblies has important implications for the elucidation of their role in natural processes such as photosynthesis, and for the control of electron migration in oligonuclear complexes designed for such applications as artificial light-harvesting.

Dinuclear ligand-bridged mixed-valence complexes, particularly of ruthenium, have been extensively studied in this context by investigations of the intervalence charge transfer (IVCT) transitions which are spectrally observed in the near-infrared (NIR) region. Theoretical treatments from Marcus [1,2] have addressed the issues of the activation barriers to intramolecular electron transfer, and Hush [3,4] has provided insights into the manner in which such processes may be probed through the IVCT transitions.

In weakly-coupled (Class II) [5] systems, the energy of the IVCT band (ν_{max}) is given by Eq. (1) [3,4]

$$\nu_{max} = \lambda_i + \lambda_o + \Delta E_0 + \Delta E' \quad (1)$$

where ΔE_0 is redox asymmetry, $\Delta E'$ includes contributions due to spin-orbit coupling and/or ligand field asymmetry, and λ represents the sum of the Franck-Condon reorganisational energies—composed of an *inner*-sphere component (λ_i) corresponding to the energy required for reorganisation of the metal-ligand and intra-ligand bond lengths and angles, and an *outer*-sphere component (λ_o) corresponding to the energy required for reorganisation of solvent and anion molecules in the surrounding medium.

For symmetrical dinuclear complexes ($\Delta E_0 = 0$) which exhibit Gaussian-shaped IVCT bands, H_{ab} (defined as the electronic coupling factor) is given by Eq. (2) [3,4], where ν_{max} is the energy of the absorption, ε_{max} is the maximum intensity of the band and $\Delta\nu_{1/2}$ is the band-width at half-height. While the electron transfer distance, r_{ab}, is often equated with the through-space geometrical distance between the metal centres, the *effective* charge transfer distance is decreased relative to the

*Corresponding author . E-mail: richard.keene@jcu.edu.au

ISSN 1061-0278 print/ISSN 1029-0478 online © 2005 Taylor & Francis
DOI: 10.1080/10610270500310537

geometric distance as electronic coupling across the bridge increases, and Eq. (2) provides a lower limit only for H_{ab} [6].

$$H_{ab} = \frac{2.06 \times 10^{-2} (\nu_{max}\, \varepsilon_{max}\, \Delta\nu_{1/2})^{1/2}}{r_{ab}} \qquad (2)$$

A more rigorous quantum mechanical formulation of Eq. (2) is given by Eq. (3) [7,8], where M is the adiabatic transition moment, r_{ab} is the distance between the diabatic (non-interacting) redox centres and e is the unit electronic charge. This form of the Eq. for H_{ab} has the advantage that no implicit assumption is made regarding the shape of the IVCT band, as M may be calculated from the integrated intensity of the absorption band.

$$H_{ab} = \frac{M}{e r_{ab}}\, \nu_{max} \qquad (3)$$

The Hush model [3,4] has provided the preferred method of analysis for mixed-valence complexes due to the ease of interpretation of the derivation and the facility of its application. The classification of mixed-valence complexes as localised (Class II), delocalised (Class III), or intermediate localised-to-delocalised systems is generally based upon the observed band-width at half-height ($\Delta\nu_{1/2}$) compared with that expected from Hush theory in the limit of a localised two-site transition ($\Delta\nu_{1/2}^{\circ}$). The validity of the classical two-state model for the determination of the relative contributions of the fundamental parameters expressed in Eqs. (1)–(3) has been extensively tested and reviewed [6,9–17]. Experimentally, these contributions have been probed by the dependence of the IVCT characteristics on structural and substitutional changes in the mixed-valence systems. These include the distance between the metal centres [9], the ability of the bridging ligand to delocalise the electronic charge [18], the coordination environments of the metal centres which are influenced by the terminal ligands and variations in the conformations or length of the bridging ligands [6,10–13,15,16]. Variations in the external environment surrounding the mixed-valence species also influence the fundamental parameters. These include changes in the identity and composition of the solvent [17,19–31], in addition to the effects of temperature [32–36], pressure [37,38] and anions in the surrounding medium [39–44]. While the classical model has been successfully applied for the analysis of complexes in the strongly localised (Class II) and delocalised (Class III) limits, apparent break-downs may occur between these two extremes [17] in the presence of specific solvent-solute interactions [45], or significant electronic delocalisation [14].

$$\Delta\nu_{1/2}^{\circ} = [16 k_B T \ln 2(\lambda_i + \lambda_0)]^{1/2}$$
$$= [16 k_B T \ln 2(\nu_{max} - \Delta E_0 - \Delta E')]^{1/2} \qquad (4)$$

According to the band-width criterion, if $\Delta\nu_{1/2} \geq \Delta\nu_{1/2}^{\circ}$ the system is localised, and if $\Delta\nu_{1/2} < \Delta\nu_{1/2}^{\circ}$ the system is delocalised. In addition, a solvent dependence of the mixed-valence band signals valence localisation, while solvent independence signals delocalisation [10,11,46]. The discrimination between the two regimes is not straightforward as band-shape analyses are frequently complicated by multiple overlapping transitions, and a significant number of mixed-valence systems exhibit the characteristics of *both* localised and fully delocalised systems.

Characterisation of the IVCT properties in mixed-valence systems therefore provides a window to the elucidation of the fundamental factors which govern the barrier to intramolecular electron transfer and the degree of delocalisation.

The redox asymmetry contributions (ΔE_0) to ν_{max} in Eq. (1) have been probed by direct structural perturbations such as variations in the identity of the peripheral ligands at one terminus in series of dinuclear ruthenium complexes [47], the incorporation of unsymmetrical bridging ligands such as bis(2-pyridyl)triazolate (bpt^-) [48–53], or the use of heteronuclear complexes of ruthenium and osmium [6]. Conformational variations in the bridging ligand structures have also been shown to introduce effective redox asymmetry contributions [13], in addition to environmental perturbations such as selective solvation effects involving H-bonding interactions with the terminal or bridging ligands [54], crown-ether encapsulation effects [26,55,56] and preferential ion-pairing with commonly employed electrolyte anions such as PF_6^- and halide anions (Cl^-, Br^-, I^-) [10,13,17]. The incorporation of redox asymmetry diminishes the electronic delocalisation and thereby induces localisation in a nominally valence-delocalised complex.

Environmental effects such as solvent and anion rearrangement, and the temperature of the medium, also constitute critical contributions to the activation barrier to electron transfer through their influence on λ_o and ΔE_0 [10,11,13,17]. In the present study, an examination of the temperature and anion dependencies of the IVCT process in the diastereoisomers of a series of structurally-related complexes provides a means to evaluate the modification of reorganisational effects and redox asymmetries induced by *subtle* and *systematic* stereochemical and substitutional changes in the complexes.

IVCT thermochromism studies on the diastereoisomers of $[\{Ru(bpy)_2\}_2(\mu\text{-BL})]^{5+}$ {BL = dpb′, dpq′,

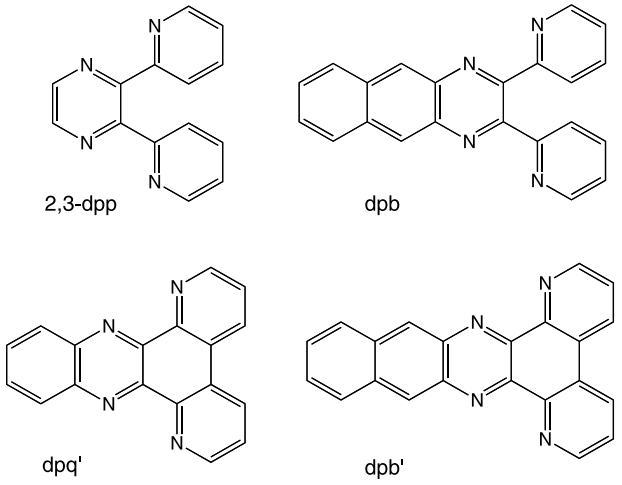

FIGURE 1 Bridging ligands.

and dpb (see Fig. 1): dpb′ = dipyrido(2,3-a;3′,2′-c) benzophenazine; dpq′ = dipyrido(2,3-a;3′,2′-c)phenazine; dpb = 2,3-bis(2-pyridyl)-1,4-benzoquinoxaline} in the presence of the weakly-ion pairing electrolyte $[(n\text{-}C_4H_9)_4N]\{B(C_6F_5)_4\}$ [57], were undertaken since the differences in the degree of electronic communication between the metal centres are related to the rate of electron transfer, and hence the temperature dependencies of the IVCT process [17]. By the comparison of the diastereoisomers based on the "fused" bridging ligands dpb′ and dpq′ with those incorporating the "unfused" ligand dpb, the subtle differences in the structural, stereochemical and electronic properties were expected to provide more detailed insights into the influence of temperature variations on the reorganisational and redox asymmetry energies [10,32–35,58–62].

Ion-pairing studies were also undertaken to investigate differential stereochemically-directed anion effects on the IVCT properties of the diastereoisomeric forms of the same series of complexes, in particular in the presence of relatively strongly (PF_6^-) and weakly $\{B(C_6F_5)_4\}^-$ ion-pairing anions [57] to provide detailed insights into ion-pairing effects on electron transfer at the molecular level [37,39–44,63,64].

EXPERIMENTAL

Materials

Lithium tetrakis(pentafluorophenyl)borate ($Li\{B(C_6F_5)_4\}.Et_2O$; Boulder Scientific) and sodium toluene-4-sulfonate (Aldrich, 98%) were used as received. Tetra-*n*-butylammonium hexafluorophosphate ($[n\text{-}C_4H_9)_4N]PF_6$; Fluka, 99 + %) was dried *in vacuo* at 60°C prior to use and ferrocene (Fc; BDH) was purified by sublimation. SP Sephadex C-25 was obtained from Amersham Pharmacia Biotech. Acetonitrile (CH_3CN; Aldrich, 99.9 + %) was distilled over CaH_2 before use and *n*-butyronitrile (Aldrich, 99 + %) was used as received. $[(n\text{-}C_4H_9)_4N]\{B(C_6F_5)_4\}$[57], was prepared by metathesis from $Li\{B(C_6F_5)_4\}.Et_2O$ as described previously [45].

Instrumentation and Physical Methods

1D and 2D ^1H NMR spectra were performed on a Varian Mercury 300 MHz spectrometer. The ^1H NMR chemical shifts for all complexes are reported relative to 99.9% d_3-acetonitrile {CD_3CN; Cambridge Isotope Laboratories (CIL)} at $\delta = 1.93$ ppm. ^1H NMR assignments were performed with the assistance of COSY experiments to identify each pyridine ring system.

Elemental microanalyses were performed at the Microanalytical Unit in the Research School of Chemistry, Australian National University.

Electrochemical measurements were performed under argon using a Bioanalytical Systems BAS 100A Electrochemical Analyser. Cyclic and differential pulse voltammograms were recorded under Ar in 0.02 M $[(n\text{-}C_4H_9)_4N]\{B(C_6F_5)_4\}/CH_3CN$ at +25°C using a glassy carbon working electrode, a platinum wire auxiliary electrode and an Ag/AgCl (0.02 M $[(n\text{-}C_4H_9)_4N]\{B(C_6F_5)_4\}/CH_3CN$) reference electrode. Ferrocene was added as an internal standard on completion of each experiment {the ferrocene/ferrocenium couple (Fc^+/Fc^0) occurred at +550 mV *vs.* Ag/AgCl}: all potentials are quoted in mV versus Fc^+/Fc^0. Cyclic voltammetry was performed with a sweep rate of 100 mV s^{-1}; differential pulse voltammetry was conducted with a sweep rate of 4 mV s^{-1} and a pulse amplitude, width and period of 50 mV, 60 ms and 1 s, respectively. Potentials from DPV experiments are reported ± 3 mV. In order to obtain reasonable electrochemical responses, measurements in the 0.02 M $[(n\text{-}C_4H_9)_4N]\{B(C_6F_5)_4\}/CH_3CN$ electrolyte required a concentration of complex approximately double that in 0.1 M $[(n\text{-}C_4H_9)_4N]PF_6/CH_3CN$.

Electronic spectra were recorded using a CARY 5E UV/Vis/NIR spectrophotometer interfaced to Varian WinUV software. The absorption spectra of the electrogenerated mixed-valence species were obtained *in situ* by the use of an Optically Semi-Transparent Thin-Layer Electrosynthetic (OSTLE) cell (path length 0.685 mm) mounted in the path of the spectrophotometer [65,66]. Solutions for the spectroelectrochemical experiments typically contained 0.1 M $[(n\text{-}C_4H_9)_4N]PF_6$ supporting electrolyte and the complex (*ca.* 1 mM) under investigation in the given solvent, while solutions for the thermochromism measurements were performed using a constant low concentration of both the complex (0.4 mM) and supporting electrolyte (0.02 M $[(n\text{-}C_4H_9)_4N]\{B(C_6F_5)_4\}$) in order to minimise inhomogeneous broadening due to ion pairing and concentration effects [36,43,44,57,64,67–69]. All solutions

were purged with N_2 prior to transference (via syringe) into the OSTLE cell. The low temperature facility enabled *in situ* spectroelectrochemical characterisation of the electrogenerated species which were otherwise unstable at room temperature. The temperature was stabilised to ± 0.3°C prior to commencing electrolysis. The dinuclear systems required approximately 6 h for data collection at -35°C.

For IVCT bands that exhibit an asymmetric appearance, application of the Eqs. derived from the classical analysis of Hush [4] is not valid as the Eqs. assume a Gaussian shape, so that an examination of the first order moments (M_1) for the electronic absorption is required for the IVCT analysis [4], rather than the experimentally observed quantities $\{\nu_{max}, \Delta\nu_{1/2}$ and $(\varepsilon/\nu)_{max}\}$. M_1 is defined as the average energy of absorption peak: in the present work, an examination of the moments to first-order (i.e. M_1) only was undertaken but it is noted that consideration of the higher order moments would be necessary in an exact treatment.

Synthesis and Stereochemistry

The ligands dpb [70], dpb′ [36,71], and dpq′ [71] were prepared as reported previously. The mononuclear ruthenium precursor *cis*-$[Ru(bpy)_2Cl_2].2H_2O$ [72] was synthesised according to literature methods.

[{Ru(bpy)$_2$}$_2$(μ-dpb)](PF$_6$)$_4$

$[\{Ru(bpy)_2\}_2(\mu\text{-dpb})](PF_6)_4$ was prepared using microwave techniques in 90% yield [70]. A sample for microanalysis was purified by passage through a short column (20 cm length × 1 cm diameter) of Sephadex LH20 (eluent 50% methanol-acetone). *Anal.* Calcd for $C_{62}H_{46}F_{24}N_{12}P_4Ru_2$: C, 42.8; H, 2.66; N, 9.65%. Found: C, 42.7; H, 2.60; N, 9.42%. Separation of the diastereroisomers was achieved by cation exchange chromatography on SP Sephadex C-25 support (column dimensions 95 × 2 cm) with 0.25 M sodium toluene-4-sulfonate solution as eluent [70]. ^{1}H NMR data for the diastereoisomers have been reported previously [36].

[{Ru(bpy)$_2$}$_2$(μ-dpb′)](PF$_6$)$_4$

$[\{Ru(bpy)_2\}_2(\mu\text{-dpb}')](PF_6)_4$ was prepared in 71% yield from dpb′ in an analogous manner to $[\{Ru(bpy)_2\}_2(\mu\text{-dpb})](PF_6)_4$ [36,70]. The dinuclear species was isolated as an olive green solid. *Anal.* Calcd for $C_{62}H_{44}F_{24}N_{12}P_4Ru_2$: C, 42.8; H, 2.55; N, 9.70%. Found: C, 42.6; H, 2.56; N, 9.65%. Separation of the diastereroisomers was achieved by cation exchange chromatography on SP Sephadex C-25 support using 0.25 M sodium toluene-4-sulfonate as eluent: ^{1}H NMR data for the diastereoisomers have been reported previously [36].

[{Ru(bpy)$_2$}$_2$(μ-dpq′)](PF$_6$)$_4$

The synthesis (yield 87%), diastereoisomeric separation and purification were performed in a similar manner to those described above for $[\{Ru(bpy)_2\}_2(\mu\text{-dpb})](PF_6)_4$ using dpq′ instead of dpd. The dinuclear species was isolated as an olive green solid. *Anal.* Calcd for $C_{58}H_{42}F_{24}N_{12}P_4Ru_2$: C, 41.2; H, 2.51; N, 10.0%. Found: C, 41.0; H, 2.48; N, 9.88%. ^{1}H NMR (δ ppm; CD_3CN): (Band 1; *meso*) 6.91 (H6d, 2H, $J = 5$, 1.5 Hz, dd), 7.15 (H5d, 2H, $J = 8$, 5 Hz, dd), 7.30 (H5b, 2H, $J = 8$, 5 Hz, dd), 7.44 (H5c, 2H, $J = 8$, 5 Hz, dd), 7.53 (H5a, 2H, $J = 8$, 5 Hz, dd), 7.56 (H2/5 dpq′, 2H, $J = 3$ Hz, d), 7.66 (H6c, 2H, $J = 5$, 1.5 Hz, dd), 7.70 (H3/4 dpq′, 2H, $J = 10$, 8 Hz, dd), 7.78 (H4d, 2H, $J = 8$, 8 Hz, dd), 7.99 (H6a/H6b, 4H, $J = 5$, 1.5 Hz, dd), (H9/12 dpq′, 2H), 8.05 (H4a, 2H, $J = 8$, 8 Hz, dd), 8.16 (H4b/H4c, 4H, $J = 8$, 8 Hz, dd), 8.16 (H8/13 dpq′, 2H), 8.19 (H4c, 2H, $J = 8$, 8 Hz, dd), 8.28 (H3a, 2H, $J = 8$, 1.5 Hz, dd), 8.68 (H3c/H3b, 4H, $J = 8$, 1.5 Hz, dd), 9.35 (H10/11 dpq′, $J = 8$, 1.5 Hz, dd); (Band 2; *rac*) 7.03 (H5b, 2H, $J = 8$, 5 Hz, dd), 7.25 (H5d, 2H, $J = 8$, 5 Hz, dd), 7.33 (H6d, 2H, $J = 5$, 1.5 Hz, dd), 7.45-7.52 (H6b/H5c/H5a, H2/5 dpq′, H3/4 dpq′, 5H, m), 7.63 (H6a, 2H, $J = 5$, 1.5 Hz, dd), 7.85 (H6c, 2H, $J = 5$, 1.5 Hz, dd), 7.98 (H9/12 dpq′, 2H, $J = 10$, 8 Hz, dd), 8.03 (H4b, 2H, $J = 8$, 8 Hz, dd), 8.07 (H4d, 2H, $J = 8$, 8 Hz, dd), 8.09 (H4c, 2H, $J = 8$, 8 Hz, dd), 8.13 (H4a, 2H, $J = 8$, 8 Hz, dd), 8.17 (H8/13 dpq′, 2H), 8.49 (H3d, 2H, $J = 8$, 1.5 Hz, dd), 8.54 (H3a/H3b, 4H, $J = 8$, 1.5 Hz, dd), 8.58 (H3c, 2H, $J = 8$, 1.5 Hz, dd), 9.31 (H10/11 dpq′, 2H, $J = 8$, 1.5 Hz, d).

X-ray Crystallography

Single crystals of *meso*-$[\{Ru(bpy)_2\}_2(\mu\text{-dpb})](PF_6)_4.5H_2O$ (1; dark red rod-shaped crystals) and *meso*-$[\{Ru(bpy)_2\}_2(\mu\text{-dpb}')](PF_6)_4.2H_2O.2\{(CH_3)_2CO\}$ (2; dichroic red/green crystals) were grown by slow evaporation of a solution of *ca.* 1 mmol of the complex in acetone/water (1:1, 2 cm^3) under ambient conditions in the absence of light.

Single crystals of *meso*-$[\{Ru(bpy)_2\}_2(\mu\text{-dpb})](ZnCl_4)_2.5H_2O$ (3) and *meso*-$[\{Ru(bpy)_2\}_2(\mu\text{-dpq}')](ZnCl_4)_2.3H_2O$ (4) were obtained by initially stirring a suspension of 10 mg of the hexafluorophosphate salt in 1 cm^3 distilled water with 0.5 g DOWEX® anion exchange resin (Cl^- form), to afford the corresponding chloride salt. Following the addition of two molar equivalents of $ZnCl_2$ and aqueous HCl (3 drops, 2 M), the solutions were allowed to evaporate slowly at room temperature to yield dichroic red/green rod-shaped crystals of 3 and 4 suitable for X-ray determination.

For compounds 1, 3 and 4, hemispheres of data were collected (capillary sealed specimens) at room

temperature on a Bruker SMART CCD diffractometer using the omega scan mode with total reflections and unique data listed below. Data sets were corrected for absorption using the program SADABS [73]. A crystalline sample of compound 2 was mounted upon a glass fibre in viscous paraffin oil at 123 K and crystal data obtained using an Enraf-Nonius Kappa CCD diffractometer. Structural solution and refinement for all structures was carried out using SHELXL-97 [74] utilising the graphical interface X-Seed [75]. All non-hydrogen atoms were located and were refined with anisotropic thermal parameters. Hydrogen atoms were placed in calculated positions (riding model) and were not refined. For 1, all four PF_6^- anions were disordered and these were successfully modelled with partial occupancies and hydrogen atoms on lattice water molecules were not located. For 3, hydrogen atoms on the water molecules were not located and all non-H atoms refined anisotropically except the water molecules, which had high thermal motion. For 4, oxygen atoms of the water molecules were isotropically refined and their hydrogen atoms were not located. For 2, oxygen atoms of the lattice water molecule and all atoms of the lattice acetone molecules were isotropically refined and the hydrogen atoms of lattice water were not located. Crystal data and a summary of data collection appear below.

Crystallographic data (excluding structure factors) for the structures reported in this paper have been deposited with the Cambridge Crystallographic Data Centre as supplementary publication no. CCDC 276213 for compound 1, CCDC 276214 for compound 2, CCDC 276215 for compound 3 and CCDC 276216 for compound 4. Copies of the data can be obtained free of charge on application to the CCDC, 12 Union Road, Cambridge, CB2 1EZ, UK (fax: (+44) 1223 336 033; . E-mail: deposit@ccdc.cam.ac.uk).

Crystal data for 1: $C_{62}H_{56}F_{24}N_{12}O_5P_4Ru_2$, M = 1831.21, 0.40 × 0.40 × 0.30 mm, orthorhombic, space group *Fdd*2 (No. 43), $a = 39.640(2)$, $b = 69.321(4)$, $c = 10.8530(6)$Å, $V = 29823(3)$Å^3, $Z = 16$, $D_c = 1.631\,g/cm^3$, $F_{000} = 14656$, Bruker SMART 1000 CCD diffractometer, MoKα radiation, $\lambda = 0.71073$ Å, $T = 296(2)$K, $2\theta_{max} = 46.6°$, 34612 reflections collected, 10479 unique ($R_{int} = 0.1089$). Final *GooF* = 0.972, *R1* = 0.0703, *wR2* = 0.1667, *R* indices based on 6456 reflections with I > 2sigma(I) (refinement on F^2), 1173 parameters, 395 restraints. Lp and absorption corrections applied, $\mu = 0.606\,mm^{-1}$. Absolute structure parameter = −0.07(6) [76].

Crystal data for 2: $C_{65}H_{50}F_{24}N_{12}O_{1.50}P_4Ru_2$, M = 1805.19, 0.30 × 0.30 × 0.20 mm, orthorhombic, space group *Pbca* (No. 61), $a = 25.283(5)$, $b = 22.151(4)$, $c = 26.204(5)$Å, $V = 14675(5)$Å^3, $Z = 8$, $D_c = 1.634\,g/cm^3$, $F_{000} = 7200$, Nonius Kappa CCD, MoKα radiation, $\lambda = 0.71073$ Å, $T = 123(2)$K, $2\theta_{max} = 56.9°$, 145604 reflections collected, 18350 unique ($R_{int} = 0.1500$). Final *GooF* = 0.889, *R1* = 0.0643, *wR2* = 0.1562, *R* indices based on 8716 reflections with I > 2sigma(I) (refinement on F^2), 977 parameters, 0 restraints. Lp and absorption corrections applied, $\mu = 0.612\,mm^{-1}$.

Crystal data for 3: $C_{62}H_{56}Cl_8N_{12}O_5Ru_2Zn_2$, M = 1665.67, 0.30 × 0.15 × 0.15 mm, monoclinic, space group $P2_1/c$ (No. 14), a = 19.608(3), b = 16.821(2), c = 20.930(3)Å, β = 96.956(3)°, V = 6852.4(16)Å^3, Z = 4, $D_c = 1.615\,g/cm^3$, $F_{000} = 3344$, Bruker SMART 1000 CCD diffractometer, MoKα radiation, λ = 0.71073 Å, T = 296(2)K, $2\theta_{max} = 46.5°$, 30784 reflections collected, 9794 unique (R_{int} = 0.1882). Final GooF = 0.826, R1 = 0.0667, wR2 = 0.1307, R indices based on 3629 reflections with I > 2sigma(I) (refinement on F^2), 795 parameters, 0 restraints. Lp and absorption corrections applied, $\mu = 1.493\,mm^{-1}$.

Crystal data for 4: $C_{58}H_{48}Cl_8N_{12}O_3Ru_2Zn_2$, *M* = 1577.56, 0.35 × 0.30 × 0.28 mm, triclinic, space group $P-1$ (No. 2), $a = 10.1847(9)$, $b = 16.3990(15)$, $c = 19.5070(17)$Å, $\alpha = 96.148(2)$,? $\beta = 104.781(2)$,? $\gamma = 96.216(2)°$, $V = 3100.8(5)$Å^3, $Z = 2$, $D_c = 1.690\,g/cm^3$, $F_{000} = 1576$, Bruker SMART 1000 CCD diffractometer, MoKα radiation, $\lambda = 0.71073$ Å, $T = 296(2)$K, $2\theta_{max} = 46.5°$, 14258 reflections collected, 8834 unique ($R_{int} = 0.0652$). Final *GooF* = 0.934, *R1* = 0.0493, *wR2* = 0.1246, *R* indices based on 6710 reflections with I > 2sigma(I) (refinement on F^2), 751 parameters, 0 restraints. Lp and absorption corrections applied, $\mu = 1.642\,mm^{-1}$.

RESULTS AND DISCUSSION

Diastereoisomer Synthesis, Separation and Structural Characterisation

The complexes $[\{Ru(bpy)_2\}_2(\mu\text{-BL})]^{4+}$ {BL = dpb, dpb′, dpq′} were synthesised by the reaction of 2.2 equivalents of *cis*-$[Ru(bpy)_2Cl_2].2H_2O$ with the bridging ligand in ethylene glycol, using the microwave-assisted methodology which is well established for a range of mono- [77–79], di- [36,70,71,79,80], and trinuclear [79,81] polypyridyl complexes of ruthenium(II) and osmium(II).

The separation of the diastereoisomeric forms of the dinuclear complexes was achieved by cation exchange chromatography using SP Sephadex C-25 as the support with aqueous 0.25 M sodium toluene-4-sulfonate solution as eluent [82]. For all three complexes the Band 1 and 2 eluates were determined to be the *meso* and *rac* diastereoisomers, respectively, as established from X-ray crystallographic and NMR characterisation (see below).

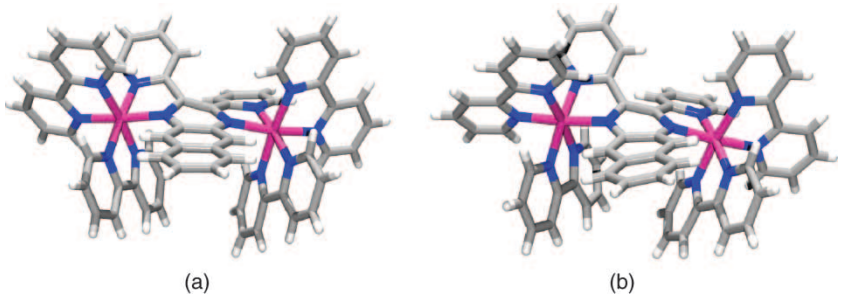

FIGURE 2 X-ray crystal structures of the cations in *meso*-[{Ru(bpy)$_2$}$_2$(μ-dpb)](PF$_6$)$_4$.5H$_2$O (**1**) and *meso*-[{Ru(bpy)$_2$}$_2$(μ-dpb)][ZnCl$_4$]$_2$.5H$_2$O (**3**), with atom labelling.

^{1}H NMR Studies

The assignment of the ^{1}H NMR spectra was performed with the assistance of 2D COSY spectra, and by comparison with the spectra of the diastereoisomers of the structurally-related complex [{Ru(bpy)$_2$}$_2$(μ-HAT)]$^{4+}$ {HAT = 1,4,5,8,9,12-hexaazatriphenylene} [81,83], for which the characterisation of the diastereoisomers has been established on the basis of distinctive ^{1}H resonances associated with differential anisotropic effects of the terminal ligands above (and below) the plane of the bridging ligand.

The diastereoisomers of [{Ru(bpy)$_2$}$_2$(μ-dpb)]$^{4+}$ exhibit broader ^{1}H NMR spectra than the [{Ru(bpy)$_2$}$_2$(μ-dpb′)]$^{4+}$ analogues. Steric interactions between the H3 and H3′ protons of the two pyridine rings of the dpb bridging ligand (Supplementary Information; Fig. S1) induce a structural distortion in the bridging ligand by forcing the pyridyl rings to move out of the plane of the bridge, which gives rise to conformational isomers that interchange slowly (on the NMR timescale) at room temperature. The resultant spectral broadening is relatively greater for the *meso* diastereoisomer compared with the *rac* form. A similar observation has been reported for the related system [{Ru(bpy)$_2$}$_2$(μ-2,3-dpp)]$^{4+}${2,3-dpp = 2,3-bis(pyridyl)pyrazine} [82]. For the diastereoisomers incorporating the "fused" bridging ligand dpb′, the rigidity precludes such conformational lability. Despite the broadening of the resonances in the complexes incorporating the "unfused" bridging dpb ligand, the diastereoisomeric forms of the complex exhibit distinctive resonances which permit their characterisation.

X-ray Crystallography

The X-ray crystal structures of the *meso*-[{Ru(bpy)$_2$}$_2$(μ-dpb)]$^{4+}$ cation were obtained as the both the PF_6^- (1) and $[ZnCl_4]^{2-}$ (3) salts. The perspective views of the two complexes (with partial atom labelling) are shown in Fig. 2. In both cases, the dpb bridging ligand exhibits a large dihedral skew of the two pyridyl ligands arising from steric hindrance (see above), as well as considerable distortion in the central pyrazine ring and a twist in the benzophenazine "tail" of the bridge. As a consequence of the dihedral skew, C(1) deviates from the least-squares plane defined by the benzoquinoxaline tail of the bridging ligand by 0.503 and 0.730 Å for the structures involving PF_6^- and $[ZnCl_4]^{2-}$ counter-anions, respectively, indicating that ion-pairing interactions between the counter-ions and cationic complex influence the degree of structural distortion in the solid-state. The two structures exhibit different Ru(1)…Ru(2) separations of 6.8826(13) and 6.8557(17)Å for the PF_6^- (1) and $[ZnCl_4]^{2-}$ (3) structures, respectively (Table I). In (1), one PF_6^- counter-ion resides in the cleft between the terminal bpy ligands "above" the plane of the bridging ligand, while the additional three counter-ions and five water molecules reside within the exterior clefts. By contrast, in (3) two $[ZnCl_4]^{2-}$ counter-ions are located

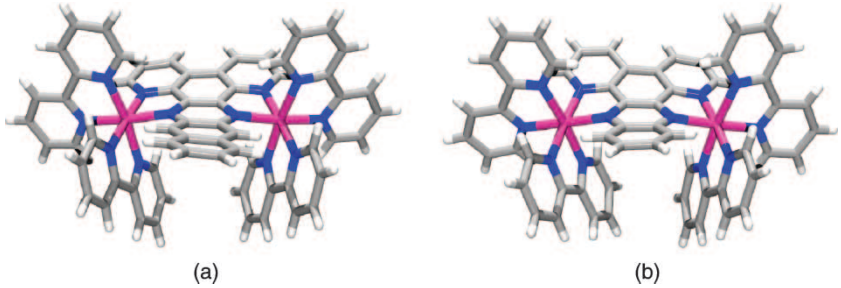

FIGURE 3 X-ray crystal structures of the cations in (a) *meso*-[{Ru(bpy)$_2$}$_2$(μ-dpb′)](PF$_6$)$_4$.2H$_2$O.2{(CH$_3$)$_2$CO} (**2**) and (b) *meso*-[{Ru(bpy)$_2$}$_2$(μ-dpq′)][ZnCl$_4$]$_2$.3H$_2$O (**4**) with atom labelling.

TABLE I Ru···Ru distances (r_{geom}) determined by X-ray analysis of the $[\{Ru(bpy)_2\}_2(\mu\text{-BL})]^{4+}$ cations

Complex		r_{geom} /Å
meso-$[\{Ru(bpy)_2\}_2(\mu\text{-dpb})]^{4+}$	(**1**)	6.8826(13)
meso-$[\{Ru(bpy)_2\}_2(\mu\text{-dpb})]^{4+}$	(**3**)	6.8557(17)
meso-$[\{Ru(bpy)_2\}_2(\mu\text{-dpb}')]^{4+}$	(**2**)	6.8869(13)
meso-$[\{Ru(bpy)_2\}_2(\mu\text{-dpq}')]^{4+}$	(**4**)	6.8181(8)

within the exterior clefts and engage in H-bonding interactions with the lattice water molecules. In both structures, the metal centres reside in distorted octahedral environments in which the "bite-angles" subtended by the Ru centres and nitrogen atoms of the bridging ligand are *ca.* 78°. The Ru-N(pyrazine) bond lengths of 2.080(10) and 2.099(10)Å for Ru(1) and Ru(2) in the $[ZnCl_4]^{2-}$ structure are slightly longer than the Ru-N(pyridine) lengths of 2.028(10) and 2.037(11)Å. A similar trend is observed for the PF_6^- structure, in which the Ru-N(pyrazine) bond lengths of 2.074(10) and 2.101(10)Å for Ru(1) and Ru(2) are slightly longer than the Ru-N(pyridine) lengths of 2.021(10) and 2.031(11)Å.

Figs. 3a and b present the perspective views of the dinuclear cations *meso*-$[\{Ru(bpy)_2\}_2(\mu\text{-dpb}')](PF_6)_4.2H_2O.2\{(CH_3)_2CO\}$ (2) and *meso*-$[\{Ru(bpy)_2\}_2(\mu\text{-dpq}')][ZnCl_4]_2.3H_2O$ (4). By comparison with the dpb ligand, the C–C bond linking the two pyridyl rings of the bridging ligand in the dpq′ and dpb′ ligands prevents the lateral movements. In (2) and (4) the dpb′ and dpq′ bridging ligands assume a slightly arched structure in each case arising from unfavourable steric interactions between the equatorial hydrogen atoms on the benzophenazine and phenazine "tails" of the bridging ligands, respectively, and the terminal bipyridine rings oriented parallel to the long axis of the bridging ligand. The N-Ru-N "bite angles" of *ca.* 78° between the bridging ligands are comparable to those in the dpb-bridged structures. For the dpb′-bridged structure, the average Ru-N(pyrazine) and Ru-N(pyridine) bond-lengths are 2.08 and 2.06 Å, while the average lengths are 2.08 and 2.07 Å, respectively, for the dpq′-bridged structure. The similarity of the Ru-N(pyrazine) and Ru-N(pyridine) bond lengths is in contrast to those observed for the distorted dpb-bridged structures. The Ru(1)...Ru(2) distances are 6.818(8) and 6.8869(13)Å for the dpq′- and dpb′-bridged structures.

In all cases, the Ru-N distances and the N-Ru-N angles correlate with those published previously for polypyridyl complexes of ruthenium [50,80,84–88].

The presence of differential structural distortions in the bridging ligand between the complexes incorporating "unfused" and "fused" ligands suggest that there may be differences in ground-state redox asymmetry contributions across the series, and between diastereoisomeric forms of the same complex. These differences may be manifested in the electrochemical and IVCT properties of the systems.

Electrochemistry

The electrochemical properties of the diastereoisomeric forms of $[\{Ru(bpy)_2\}_2(\mu\text{-BL})]^{4+}$ {BL = dpb, dpb′, dpq′} were investigated by cyclic and differential pulse voltammetry in acetonitrile containing 0.1 M $[(n\text{-}C_4H_9)_4N]PF_6$, and are summarised in Table II. Some details of the redox and spectral characteristics of the diastereoisomers of the species containing dpb and dpb′ have been published previously [36,70,71,89–92].

All complexes are characterised by two reversible one-electron redox processes corresponding to successive oxidation of the metal centres, in addition to multiple reversible ligand-based reductions. In the cathodic region, the first two reduction processes are assigned to the successive one-electron reduction of the bridging ligands ($BL^{0/-}$ and $BL^{-/2-}$), consistent with the stronger π-acceptor nature of the bridging relative to the terminal ligands [89–92]. The subsequent four one-electron reduction processes correspond to successive reduction of the terminal bpy ligands.

Measurable differences in the ΔE_{ox} values are evident between the different complexes and between the diastereoisomeric forms of the same complex: a summary of ΔE_{ox} and the resultant K_c [10] values is provided in Table II. The magnitude of ΔE_{ox} increases as BL is varied through the series dpb, dpq′ and dpb′ and the largest difference between the ΔE_{ox} values for the diastereoisomers of the same complex is observed for $[\{Ru(bpy)_2\}_2(\mu\text{-dpb})]^{4+}${14 (±6) mV} [36,70,71]. However, a recent publication has noted the caution required in the interpretation of the relative magnitudes of the ΔE_{ox} values due to contributions from ion-pairing interactions [93].

Electronic Spectroscopy

The Uv/Vis/NIR spectral data for the un-oxidised (+4), mixed-valence (+5) and fully-oxidised (+6) forms of the three dinuclear systems (for the range 3050–30000 cm^{-1}) are reported in Supplementary Information Table SI and the spectra of the respective *meso* diastereoisomers are presented in Fig. 4.

The spectra of the un-oxidised (+4) states of the dinuclear complexes incorporating the dpb [36,71,89–92,94,95] and dpq′ [96] bridging ligands have been completely assigned previously on the basis of electrochemical, spectral and computational calculations. In the present study, the spectra for the full series of complexes are characterised by a combination of overlapping $d\pi(Ru^{II}) \rightarrow \pi^*(BL)$ and $d\pi(Ru^{II}) \rightarrow \pi^*(bpy)$ singlet metal-to-ligand (^{1}MLCT) transitions. The lowest energy absorption

TABLE II Electrochemical data (in mV relative to the Fc^+/Fc^0 couple) for the metal-based redox processes in the angular bridged dinuclear complexes $[\{Ru(bpy)_2\}_2(\mu\text{-BL})]^{4+}$ in 0.1 mol dm^{-3} $[(n\text{-}C_4H_9)_4N]PF_6/CH_3CN$

BL	Diastereo-isomer	K_c ($\times 10^{-3}$)	ΔE_{ox}	$E_{ox(2)}$	$E_{ox(1)}$	E_{red1}	E_{red2}	E_{red3}	E_{red4}	E_{red5}	E_{red6}
dpb	*meso*	2.06	196	1280	1084	−624	−1268	−1888	−2116	−2240	−2552
	rac	0.944	176	1280	1104	−624	−1260	−1876	[a]	−2252	−2640
dpb′	*meso*	8.35	232	1300	1068	−496	−1128	−1868	−1981	−2144	−2272
	rac	6.11	224	1304	1080	−464	−1116	−1888	−2180	−2716	
dpq′	*meso*	2.40	200	1285	1085	−596	−1332	−1900	−2178	−2203	
	Rac	2.40	200	1297	1097	−592	−1268	−1956	−2177	−2240	

[a] Processes complicated by adsorption/desorption peaks.

band shifts to the red as BL is varied through the series dpb, dpq′ and dpb′, consistent with the increasing stabilisation of the BL-based π* orbitals.

Spectroelectrochemical generation of the +5 and +6 forms of the diastereoisomers revealed stable isosbestic points in the spectral progressions accompanying both oxidation processes. The ^{1}MLCT absorption bands decreased in intensity following one-electron oxidation and collapsed completely following oxidation to the +6 species. The first oxidation process was characterised by the appearance of an intense new band in the region 3500–9000 cm^{-1} which collapsed completely on removal of the second electron: on this basis the band was assigned as an IVCT transition. The assignment of this band as a ligand-to-metal charge transfer transition (LMCT) transition was excluded

TABLE SI UV-visible-NIR spectral data for the dinuclear complexes $[\{Ru(pp)_2\}_2(\mu\text{-BL})]^{4+}$ (BL = dpb, dpb′ and dpq′) in 0.1 M $[(n\text{-}C_4H_9)_4N]PF_6/CH_3CN$ at −35°C. The parameters of the IVCT transitions are indicated in bold type. Errors in ν_{max} and $(\varepsilon/\nu)_{max}$ are ±10 cm^{-1} and ±0.0001/M^{-1}

BL		dpb		dpb′		dpq′	
Diastereoisomer	*n*+	ν_{max} /cm^{-1}	$(\varepsilon/\nu)_{max}$ /M^{-1}	ν_{max} /cm^{-1}	$(\varepsilon/\nu)_{max}$ /M^{-1}	ν_{max} /cm^{-1}	$(\varepsilon/\nu)_{max}$/M^{-1}
Meso	4	*sh* 13070	0.2958	*sh* 11670	0.2646	*Sh* 12900	0.2813
		15530	1.4440	13880	2.0415	15150	1.9723
		23520	1.0810	16900	0.2133	18110	0.1567
		24460	0.9824	24780	1.3524	23480	0.8393
		26870	1.5690	29140	1.5091	26690	1.0829
		29450	1.4350				
	5	**5205**	**0.3062**	**5285**	**0.8084**	**5194**	**0.5934**
		15120	0.7678	9253	0.0998	14900	1.4369
		sh 17370	0.4504	11420	0.3598	25730	1.0688
		25920	1.4740	13930	0.9596		
				21660	0.3788		
				22770	0.4739		
				24760	0.7086		
				28040	1.2751		
	6	~15000		14210	0.1497		
		16870	0.2253	20850	0.8348		
		25230	1.2709	22140	0.7751		
				27440	1.5330		
Rac	4	*sh* 13070	0.2269	*sh* 11770	0.2532	*sh* 13090	0.4341
		15420	1.4152	13870	1.8962	15290	1.9334
		20480	0.3499	16850	0.1661	18280	0.1602
		23470	1.1100	24780	1.2155	23370	0.8662
		sh 24400	0.9878	29150	1.3248	26720	1.0949
		26820	1.4918				
		29400	1.5252				
	5	**4998**	**0.4572**	**5290**	**0.7222**	**5223**	**0.6329**
		14980	0.6835	9223	0.0878	14980	1.2244
		25700	1.6362	11250	0.2793	25840	0.8573
				13920	0.9050		
				21630	0.3490		
				22680	0.4360		
				24570	0.6573		
				27980	1.1377		
	6	17760	0.1270	12730	0.3188	14450	0.2372
		25170	1.9485	15880	0.2005	21330	0.3455
				20850	0.6463	23560	0.6253
				22180	0.6198		
				27430	1.3068		

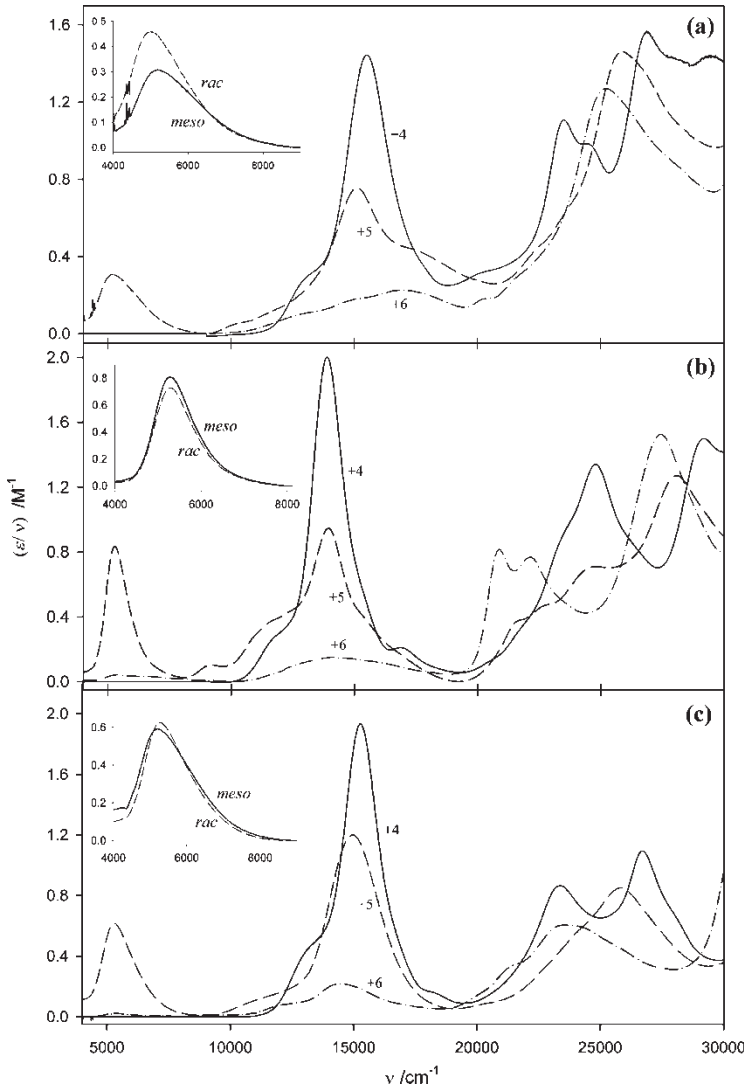

FIGURE 4 UV/Vis/NIR spectra of the reduced absorption spectra {(ε/ν) *vs.* ν} of (a) *meso*-[{Ru(bpy)$_2$}$_2$(μ-dpb)]$^{n+}$, (b) *meso*-[{Ru(bpy)$_2$}$_2$(μ-dpb′)]$^{n+}$ and (c) *meso*-[{Ru(bpy)$_2$}$_2$(μ-dpq′)]$^{n+}$ at −35°C. Insets: overlay of the IVCT bands for the *meso* and *rac* diastereoisomers.

on the basis of the lack of absorption bands in the NIR region for the +6 species, and the corresponding mononuclear complexes [Ru(bpy)$_2$(BL)]$^{3+}$ {BL = dpb and dpb′}[97].

Intervalence Charge Transfer

An overlay of the IVCT bands for the full series of complexes [{Ru(bpy)$_2$}$_2$(μ-BL)]$^{5+}$ {BL = dpb, dpb′, dpq′} in the presence of PF_6^- electrolyte is shown in Fig. 5, and the results of the band maxima (ν_{max}), molar extinction coefficients {$(\varepsilon/\nu)_{max}$}, bandwidths ($\Delta\nu_{1/2}$) of the IVCT bands (scaled as $\int\varepsilon(\nu)/\nu\,d\nu$ [3,98]) are summarised in Supplementary Information Table SII. For all complexes, the bands appear asymmetrical and narrower on the lower energy side. A moment analysis of the IVCT bands was pursued [3,98], and the results to first-order moment analysis are also presented in Table SII, where the zeroth (M_0) and first (M_1) moments represent the band area and average band energy, respectively, and M is the transition moment [4]. The electronic coupling parameter, H_{ab} is determined from Eq. (3) where r_{ab} is equated with the through-space geometrical distance between the metal centres [6] determined from the X-ray crystal structures of the complexes incorporating the dpb (average of the distances for the structures involving PF_6^- and $[ZnCl_4]^{2-}$ counter-anions of 6.870 Å), dpb′ and dpq′ bridging ligands (Table I).

In terms of a classical analysis, by comparison with the theoretical bandwidths ($\Delta\nu_{1/2}^{\circ}$) estimated on the basis of the classical two-state theory [9] [Eq. (4), where 16RTln(2) = 1836 cm^{-1} at 238 K], the relatively narrow bandwidths observed are indicative of significant electronic communication between the metal centres. The parameter Γ provides a criterion

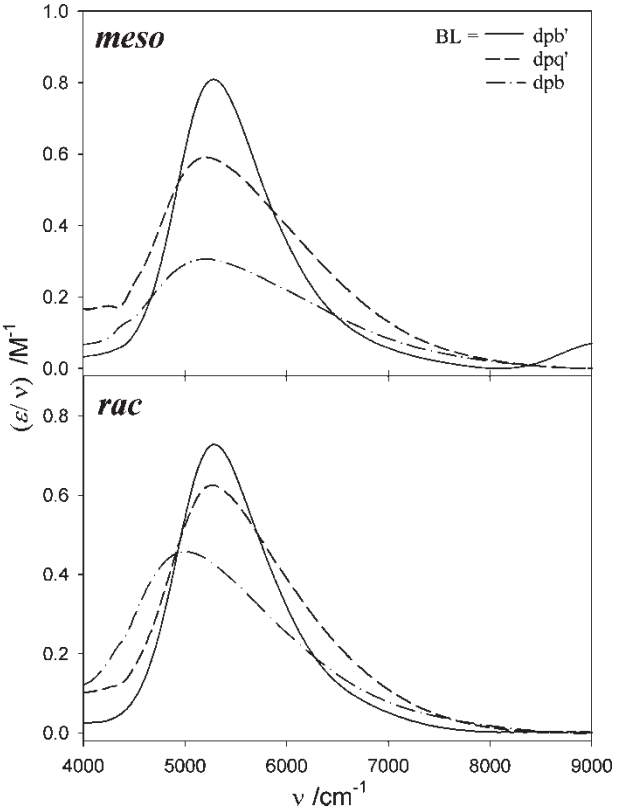

FIGURE 5 Overlay of the IVCT bands in CH_3CN for the angular bridging ligands for *meso* and *rac*[{Ru(bpy)$_2$}$_2$(μ-BL)]$^{5+}$ {BL = dpb, dpb′ and dpq′} in 0.1 M [(*n*-C_4H_9)$_4$N]PF_6^- /CH_3CN at −35°C.

for describing the degree of electronic coupling in the system [99]:

$$\Gamma = 1 - (\Delta\nu_{1/2(\exp)})/[16RT\ln(2)\nu_{\max}]^{1/2}$$
$$= 1 - (\Delta\nu_{1/2(\exp)})/(\Delta\nu_{1/2}^{\circ}) \quad (5)$$

where $0 < \Gamma < 0.5$ for weak to moderate coupling (localised Class II systems), $\Gamma \approx 0.5$ at the Class II-III transition, and $\Gamma > 0.5$ for strongly-coupled (delocalised Class III) systems. For the *meso* diastereoisomers, Γ increases as BL is varied from dpb, dpq′ to dpb′, while for both diastereoisomers of a given complex $(\varepsilon/\nu)_{max}$, $\Delta\nu_{1/2(exp)}$, *M*, M_0 and H_{ab} increase as BL is varied through the series dpb, dpb′, and dpq′ (Table SII). The results suggest that all the systems lie close to the localised-delocalised transition. For the series of fused ligands, the extent of delocalisation is most adequately assessed from the results of the moment analysis (given the asymmetrical appearance of the bands), so that the general trend is an increased extent of delocalisation as BL is varied from dpb′ to dpq′.

In the present study, the IVCT parameters suggest a marginally greater degree of delocalisation for the *meso* diastereoisomers relative to the corresponding *rac* forms, with the diastereoisomers of [{Ru(bpy)$_2$}$_2$(μ-dpb)]$^{5+}$ exhibiting the most pronounced differ-

TABLE SII IVCT spectral data of the reduced absorption spectra (ε/ν *vs.* ν) for the diastereoisomeric forms of [{Ru(bpy)$_2$}$_2$(μ-BL)]$^{5+}$ {BL = dpb, dpb′ and dpq′} at −35°C in 0.1 M [(*n*-C_4H_9)$_4$N]PF_6/CH_3CN and parameters derived from the moment analysis of the IVCT transitions

Complex	$\nu_{max} \pm 10/cm^{-1}$	$(\varepsilon/\nu)_{max} \pm 0.0001/M^{-1}$	$\Delta\nu_{1/2(exp)} \pm 10/cm^{-1}$	M_0/M^{-1}	M_1/cm^{-1}	M/eÅ	$\Delta\nu_{1/2}^{\circ}/cm^{-1}$	H_{ab} /cm^{-1}	Γ
meso-[{Ru(bpy)$_2$}$_2$(μ-dpb)]$^{5+}$	5205	0.3062	1910	639.8	5655	0.5211	3090	395	0.382
rac-[{Ru(bpy)$_2$}$_2$(μ-dpb)]$^{5+}$	5000	0.4572	1740	870.5	5450	0.6078	3030	440	0.426
meso-[{Ru(bpy)$_2$}$_2$(μ-dpb′)]$^{5+}$	5285	0.8084	1070	1010	5510	0.6546	3115	500	0.657
rac-[{Ru(bpy)$_2$}$_2$(μ-dpb′)]$^{5+}$	5290	0.7222	1080	903.2	5510	0.6190	3115	475	0.653
meso-[{Ru(bpy)$_2$}$_2$(μ-dpq′)]^5	5195	0.5934	1710	1140	5600	0.6955	3090	530	0.447
rac-[{Ru(bpy)$_2$}$_2$(μ-dpq′)]$^{5+}$	5220	0.6329	1450	1050	5600	0.6675	3100	510	0.532

ences in the observed band parameters. For example, while the IVCT energies (ν_{max} or M_1) are identical within experimental error for the diastereoisomers incorporating the series of fused bridges, the dpb-bridged diastereoisomers exhibit a 205 cm^{-1} difference in energies. The dpb-bridged diastereoisomers also exhibited the most pronounced difference in the ΔE_{ox} values for the series of complexes. The results suggest that the extent of delocalisation is dependent on the degree of structural distortion in the bridging ligand: delocalisation is enhanced for complexes incorporating smaller, less sterically-hindered bridging ligands. The extent of delocalisation differs for the diastereoisomeric forms of the same complex, the difference being more pronounced in the presence of differential structural distortions between the diastereoisomers, as is the case for the dpb-bridged species.

Differential Ion-Pairing in the Diastereoisomers of $[\{Ru(bpy)_2\}_2(\mu\text{-BL})]^{5+}$ {BL = dpb, dpb′ and dpq′}

A comparison of the IVCT bands for the diastereoisomers of $[\{Ru(bpy)_2\}_2(\mu\text{-BL})]^{5+}$ in 0.1 M $[(n\text{-}C_4H_9)_4N]PF_6$ and 0.02 M $[(n\text{-}C_4H_9)_4N]\{B(C_6F_5)_4\}$ electrolytes in acetonitrile solution at −35°C is provided in Fig. 6. An overlay of the IVCT bands for the series of complexes in 0.02 M $[(n\text{-}C_4H_9)_4N]\{B(C_6F_5)_4\}/CH_3CN$ is shown in Fig. 7, and the corresponding band parameters in that medium are summarised in Supplementary Table SIII.

The trends in the IVCT band parameters for the series of complexes in the presence of $\{B(C_6F_5)_4\}^-$ differ from those reported previously in PF_6^- media. In general, the IVCT bands are narrower for the full series of complexes in the $\{B(C_6F_5)_4\}^-$ electrolyte, and the parameters $(\varepsilon/\nu)_{max}$, M, M_0 and H_{ab} are decreased for all species except *meso*-$[\{Ru(bpy)_2\}_2(\mu\text{-dpb})]^{5+}$. The bands are red-shifted for the dpb- and dpb′-bridged diastereoisomers, and blue-shifted for the dpq′-bridged diastereoisomers relative to their positions in PF_6^- electrolyte. For $[\{Ru(bpy)_2\}_2(\mu\text{-BL})]^{5+}$ {BL = dpq′, dpb′}, small differences are observed in the IVCT energies between the diastereoisomers of the same complex. The difference of 205 cm^{-1} between the IVCT energies for the diastereoiosmers of $[\{Ru(bpy)_2\}_2(\mu\text{-dpb})]^{5+}$ in PF_6^- electrolyte (Table SII) is maintained in $\{B(C_6F_5)_4\}^-$ media, where ν_{max} and M_1 differ by 135 and 487 cm^{-1}, respectively. The Γ parameter exhibits the same trend in both electrolytes: for the *meso* diastereoisomers, Γ increases as BL is varied from dpq′ to dpb to dpb′, while Γ increases as BL is varied from dpb to dpq′ to dpb′ for the *rac* forms. The results suggest that the systems lie close to the localised-to-delocalised transition.

The significant difference in the IVCT energies between the diastereoisomers of $[\{Ru(bpy)_2\}_2(\mu\text{-dpb})]^{5+}$ is consistent with the presence of a differential redox asymmetry contribution. It would also appear that the difference is dependent on the identity of the counter-ion, which may influence the degree of structural distortion. Indeed, the presence of ion-pairing induced structural distortions between the diastereoisomeric forms occurs in the different solid-state structures of the *meso* diastereoisomer with PF_6^- and $[ZnCl_4]^{2-}$ counter-ions. The dependence of the IVCT characteristics on the identity of the electrolyte anion for the diastereoisomers of the dpq′- and dpb′-bridged complexes, which exhibit relatively less structural distortion, suggests that ion-pairing has additional fundamental microscopic consequences on the factors which contribute to the activation barrier for electron transfer [Eq. (1)].

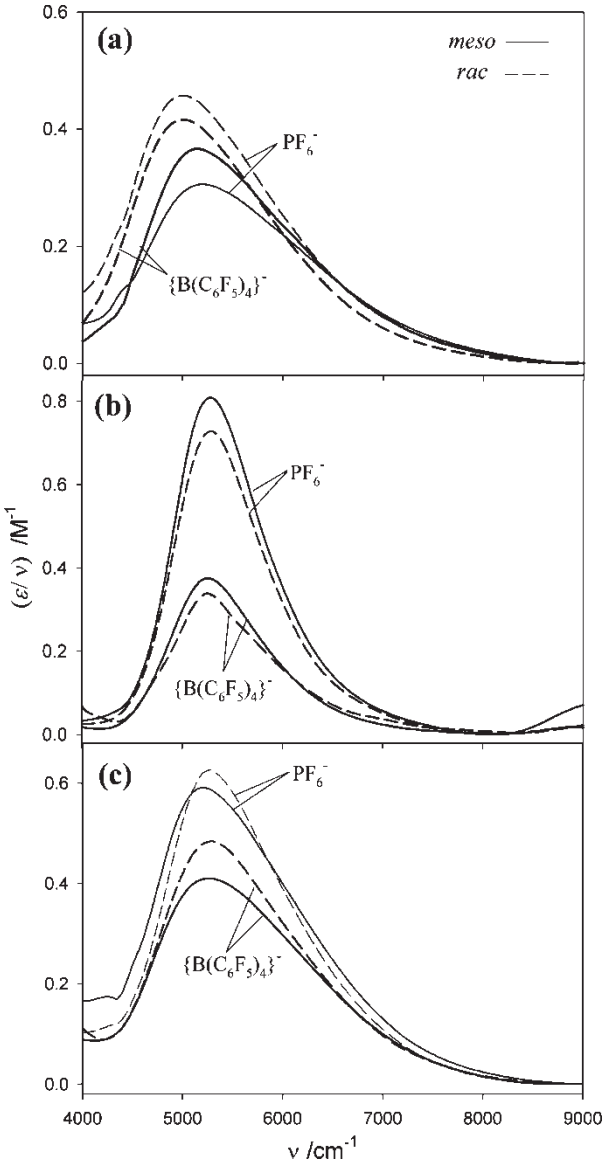

FIGURE 6 Overlay of IVCT bands in 0.1 M $[(n\text{-}C_4H_9)_4N]PF_6$ and 0.02 M $[(n\text{-}C_4H_9)_4N]\{B(C_6F_5)_4\}/CH_3CN$ electrolytes for the diastereoisomeric forms of $[\{Ru(bpy)_2\}_2(\mu\text{-BL})]^{5+}$ {BL = dpb (a), dpb′ (b) and dpq′ (c)} at −35°C.

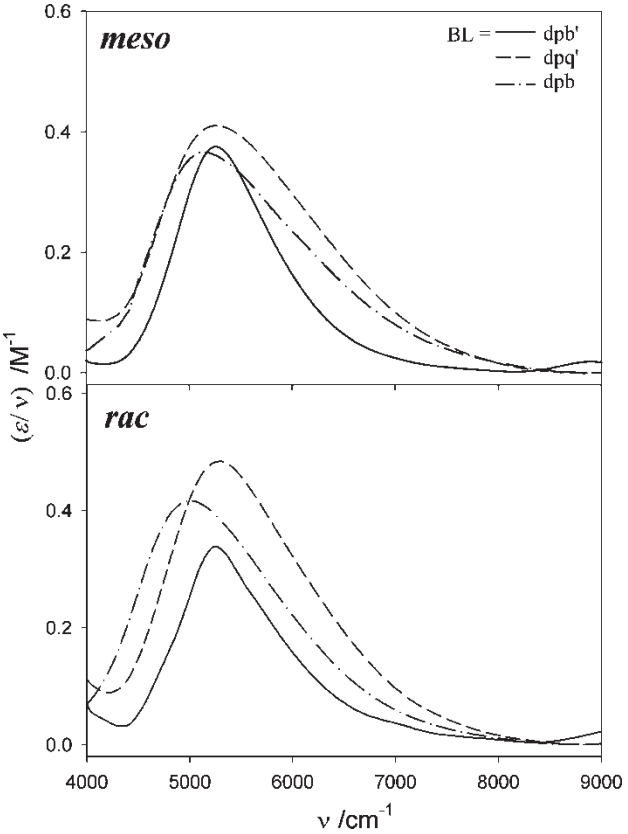

FIGURE 7 Overlay of the IVCT bands in CH_3CN for *meso*- and *rac*-$[\{Ru(bpy)_2\}_2(\mu\text{-BL})]^{5+}$ {BL = dpb, dpb′ and dpq′} in 0.02 M $[(n\text{-}C_4H_9)_4N]\{B(C_6F_5)_4\}/CH_3CN$ at −35°C.

While the dependence of the IVCT parameters on the identity of the electrolyte anion is unexpected on the basis of Eq. (1), ion-atmosphere effects have previously been shown to influence the IVCT energies and band-widths [32,41,43,44,63,69]. Qualitatively, the experimental observations in the present study are similar to previous literature reports: the addition of the relatively strongly ion-pairing electrolyte PF_6^- is accompanied by blue shifts in the IVCT bands. Alternatively, the increase in ν_{max} with increasing ionic strength has been linked to an additional reorganisational energy component due to translation of the counter-ion between the donor and acceptor [17].

IVCT thermochromism measurements for the diastereoisomeric forms of this series of complexes offer additional insights into ion-pairing, and temperature-dependent effects on the IVCT transitions. In previous studies [32–34,58,61,100], the analysis of IVCT thermochromism data has focussed on the observed energies and band-widths: the present report additionally addresses the temperature dependence of the first moment [17].

IVCT Thermochromism

A comparative study of the IVCT thermochromism of the diastereoisomers of $[\{Ru(bpy)_2\}_2(\mu\text{-dpb})]^{5+}$

TABLE SIII IVCT spectral data of the reduced absorption spectra (ε/ν *vs.* ν) for the diastereoisomeric forms of $[\{Ru(bpy)_2\}_2(\mu\text{-BL})]^{5+}$ {BL = dpb, dpb′ and dpq′} at −35°C in 0.02 M $[(n\text{-}C_4H_9)_4N]\{B(C_6F_5)_4\}/CH_3CN$ and parameters derived from the moment analysis of the IVCT transitions

Complex	ν_{max} ± 10/cm^{-1}	$(\varepsilon/\nu)_{max}$ ± 0.0001/M^{-1}	$\Delta\nu_{1/2(exp)}$ ± 10/cm^{-1}	M_0/M^{-1}	M_1/cm^{-1}	M/eÅ	$\Delta\nu_{1/2}°$/cm^{-1}	H_{ab}[a]/cm^{-1}	Γ
Meso-$[\{Ru(bpy)_2\}_2(\mu\text{-dpb})]^{5+}$	5125	0.3668	1720	688	5615	0.5403	3070	403	0.440
Rac-$[\{Ru(bpy)_2\}_2(\mu\text{-dpb})]^{5+}$	4990	0.4206	1635	753	5130	0.5653	3026	410	0.460
meso-$[\{Ru(bpy)_2\}_2(\mu\text{-dpb′})]^{5+}$	5250	0.3928	1050	470	5495	0.4466	3105	340	0.662
rac-$[\{Ru(bpy)_2\}_2(\mu\text{-dpb′})]^{5+}$	5295	0.3000	1250	460	5540	0.4418	3118	340	0.599
meso-$[\{Ru(bpy)_2\}_2(\mu\text{-dpq′})]^{5}$	5230	0.4182	1755	802	5645	0.5834	3100	447	0.434
rac-$[\{Ru(bpy)_2\}_2(\mu\text{-dpq′})]^{5+}$	5265	0.4979	1565	871	5630	0.6080	3110	470	0.496

[a] H_{ab} determined from Eq. (3), where r_{ab} is equated with the Ru···Ru distances from Table I. For BL = dpb, r_{ab} is taken as the average Ru···Ru distance of 6.870 Å from the structures involving PF_6^- and $[ZnCl_4]^{2-}$ counter-anions.

was performed in *n*-butyronitrile containing 0.1 M $[(n\text{-}C_4H_9)_4N]PF_6$ and 0.02 M $[(n\text{-}C_4H_9)_4N]\{B(C_6F_5)_4\}$. The results for the IVCT parameters are presented in Fig. 8 and Supplementary Tables SIV and SV.

As shown in Fig. 8, the energies of the IVCT bands for the diastereoisomeric forms of $[\{Ru(bpy)_2\}_2(\mu\text{-dpb})]^{5+}$ exhibit different temperature dependencies in the presence of PF_6^- and $\{B(C_6F_5)_4\}^-$, which also differ between the diastereoisomeric forms of the complex. The energies of the IVCT maxima, ν_{max}, for the *rac* diastereoisomers are relatively insensitive to temperature ($d\nu_{max}/dT = 0.41 \pm 0.24\,cm^{-1}K^{-1}$ in PF_6^- and $0.40 \pm 0.14\,cm^{-1}K^{-1}$ $\{B(C_6F_5)_4\}^-$), and the band is blue shifted by $30\,cm^{-1}$ in the presence of PF_6^-. For the *meso* diastereoisomers, ν_{max} exhibits a red shift with increasing temperature in PF_6^- electrolyte, compared with a blue shift in $\{B(C_6F_5)_4\}^-$ electrolyte ($d\nu_{max}$/-

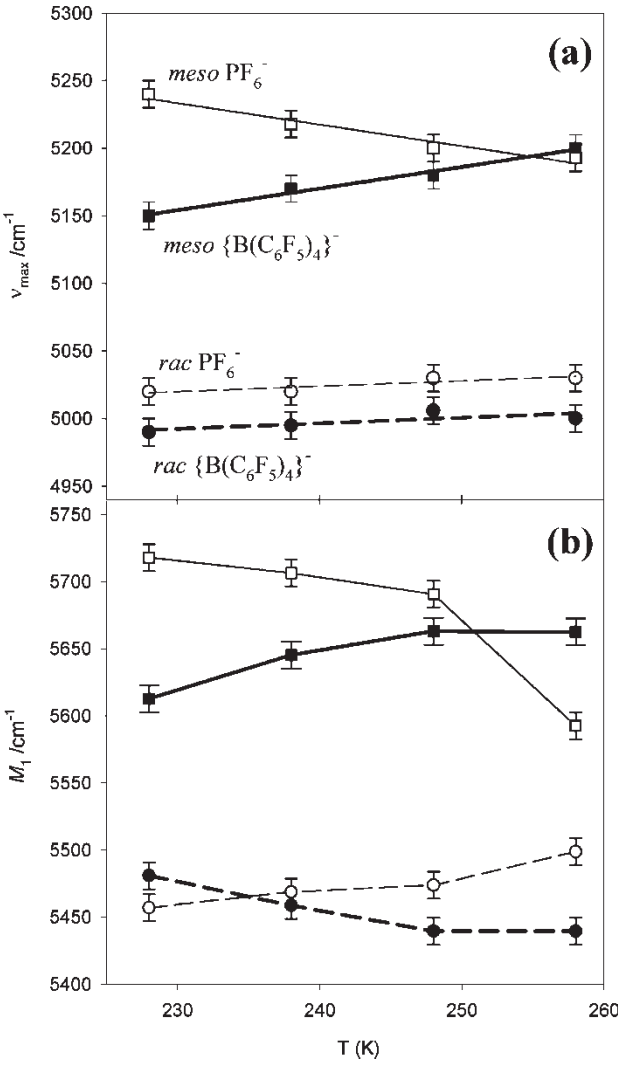

FIGURE 8 Temperature dependence of (**a**) ν_{max} and (**b**) M_1 for the *meso* (—) and *rac* (--) diastereoisomers of $[\{Ru(bpy)_2\}_2(\mu\text{-dpb})]^{5+}$ in 0.1 M $[(n\text{-}C_4H_9)_4N]PF_6$ and 0.02 M $[(n\text{-}C_4H_9)_4N]\{\{B(C_6F_5)_4\}$/*n*-butyronitrile over the temperature range −45°C (228 K) to −15°C (258 K).

TABLE SIV IVCT thermochromism data of the reduced absorption spectra (ε/ν *vs.* ν) for the diastereoisomers of $[\{Ru(bpy)_2\}_2(\mu\text{-dpb})]^{5+}$ in 0.1 M $[(n\text{-}C_4H_9)_4N]PF_6$/*n*-butyronitrile

	meso					*rac*				
T/K	$\nu_{max} \pm 10\,/cm^{-1}$	$(\varepsilon/\nu)_{max} \pm 0.0001\,/M^{-1}$	$\Delta\nu_{1/2} \pm 10/cm^{-1}$	M_0/M^{-1}	M_1/cm^{-1}	$\nu_{max} \pm 10\,/cm^{-1}$	$(\varepsilon/\nu)_{max} \pm 0.0001\,/M^{-1}$	$\Delta\nu_{1/2} \pm 10/cm^{-1}$	M_0/M^{-1}	M_1/cm^{-1}
228	5240	0.3273	2349	798.0	5718	5020	0.3372	1833	664	5457
238	5218	0.3519	1880	706.2	5707	5020	0.3874	1701	741	5469
248	5200	0.2840	1915	588.0	5691	5030	0.3637	1687	609	5474
258	5193	0.2744	1803	538.0	5593	5030	0.3607	1701	665	5499

TABLE SV IVCT thermochromism data of the reduced absorption spectra (ε/ν *vs.* ν) for the diastereoisomers of $[\{Ru(bpy)_2\}_2(\mu\text{-dpb})]^{5+}$ in 0.02 M $[(n\text{-}C_4H_9)_4N]\{B(C_6F_5)_4\}$/*n*-butyronitrile

	meso					*rac*				
T/K	$\nu_{max} \pm 10$ /cm^{-1}	$(\varepsilon/\nu)_{max} \pm 0.0001$ /M^{-1}	$\Delta\nu_{1/2} \pm 10$/cm^{-1}	M_0/M^{-1}	M_1/cm^{-1}	$\nu_{max} \pm 10$ /cm^{-1}	$(\varepsilon/\nu)_{max} \pm 0.0001$ /M^{-1}	$\Delta\nu_{1/2} \pm 10$/cm^{-1}	M_0/M^{-1}	M_1/cm^{-1}
228	5150	0.1620	1748	302	5610	4990	0.3293	1683	610	5480
238	5170	0.2673	1745	493	5645	4995	0.3698	1677	680	5460
248	5180	0.3384	1825	666	5665	5006	0.3712	1641	671	5440
258	5200	0.2588	1814	507	5660	5000	0.2621	1613	465	5440

$dT = -1.59 \pm 0.24\,cm^{-1}K^{-1}$ in PF_6^- and $1.60 \pm 0.14\,cm^{-1}K^{-1}$ $\{B(C_6F_5)_4\}^-$). Accordingly, the *meso* diastereoisomer exhibits a redox asymmetry variation with temperature whereas the *rac* form does not.

The difference between the diastereoisomers in the two electrolytes is striking, both qualitatively and quantitatively. An examination of the temperature dependencies of the first moments [17] reveal weak temperature dependencies for both diastereoisomers, as shown in Fig. 8b. The band-widths for the *rac* diastereoisomers decrease slightly with increasing temperature in both electrolytes, while the *meso* form exhibits a decrease in $\Delta\nu_{1/2(exp)}$ in PF_6^- compared with a slight increase in $\{B(C_6F_5)_4\}^-$ electrolyte.

Hupp and Dong [33] have addressed the IVCT thermochromism for localised and delocalised mixed-valence systems by considering the semi-classical adiabatic two-state treatment [95],

$$\nu_{max} = [(\lambda_i + \lambda_o + \Delta E_0 + \Delta E')^2 + 4H_{ab}^2]^{1/2} \quad (6)$$

Assuming that λ_i, λ_o and H_{ab} are temperature independent quantities [33], the temperature dependence of ν_{max} is given by $d(\Delta E_0)/dT$ in the localised limit (i.e. $\lambda_i + \lambda_o + \Delta E_0 + \Delta E' \gg 2H_{ab}$), but should approach zero in the delocalised limit (i.e. $\lambda_i + \lambda_o + \Delta E_0 + \Delta E' \ll 2H_{ab}$), regardless of the magnitude of $d(\Delta E_0)/dT$. In the localised limit, the band-width, $\Delta\nu_{1/2}$ is given by Eq. (4) [3,4]. Thus, $\Delta\nu_{1/2(exp)} \propto T^{1/2}$ and and $\Delta\nu_{1/2(exp)}$ should decrease with decreasing temperature. IVCT thermochromism measurements have been used as an argument for localisation/delocalisation [33].

In the present case, the relative invariance of ν_{max} and $\Delta\nu_{1/2(exp)}$ for the *rac* diastereoisomer in both electrolytes is suggestive of a near-delocalised classification for the mixed-valence complex. By comparison, the significantly greater temperature dependence of the *meso* form in both electrolytes suggests a greater degree of localisation, and a temperature dependence of the redox asymmetry. Two sources of redox asymmetry arise from structural asymmetry and ion-pairing asymmetry [43,44,101–103]. The latter is more pronounced at lower temperatures, and is greater for the *meso* compared with the *rac* diastereoisomeric form.

An additional possibility for rationalising the temperature dependence of the dpb-bridged diastereoisomers is the presence of conformational isomers, the proportions of which differ with temperature. The presence of conformers which will be manifest as different IVCT bands which differ with temperature, and overlap. This may explain the bandwidth variation for the *meso* diastereoisomer. If the structurally-induced redox asymmetry is a temperature invariant quantity, then the intercept (at $T = 0\,K$) gives the energy difference between the bands arising from the

structural variations [$= \nu_{max}$(*rac-meso*)] as 142 ± 34 cm^{-1}. The origin of the remaining temperature-dependent component may arise from a combination of any of the abovementioned factors.

Figures 9, 10, S2 and S3 show the variation in the IVCT energies and band-widths for the diastereoisomers of $[\{Ru(bpy)_2\}_2(\mu\text{-BL})]^{5+}$ {BL = dpb, dpb′, dpq′}, and Table SIII reports the IVCT parameters for the series of complexes in 0.02 M $\{B(C_6F_5)_4\}^-$/*n*-butyronitrile. The examination of the complexes incorporating the relatively more rigid ligands dpb′ and dpq′ also permits an assessment of the thermochromic effect on the degree of delocalisation for the systems that lie in the localised-to-delocalised regime.

As shown in Figs. 10, S2 and S3, the temperature dependencies of the IVCT parameters differ between the series of complexes, and between the diastereoisomeric forms of the same complex. The parameters ν_{max} and $\Delta\nu_{1/2(exp)}$ for the diastereoisomers of $[\{Ru(bpy)_2\}_2(\mu\text{-dpb}')]^{5+}$ exhibit a negligible temperature dependence, which is consistent with the delocalised classification for the complex, although a 100 cm^{-1} difference is maintained between the diastereoisomers over the temperature range examined. For *meso*-$[\{Ru(bpy)_2\}_2(\mu\text{-dpq}')]^{5+}$, ν_{max} is invariant with temperature, while ν_{max} shifts to the red with increasing temperature for the *rac* form $\{d\nu_{max}/dT = -1.22 \pm 0.31\ cm^{-1}K^{-1}\}$.

Hupp and co-workers [33] have shown that the IVCT bands for unsymmetrical Class II complexes shift to higher energy with decreasing temperature. The effect arises predominantly from the temperature dependence of the redox asymmetry term ΔE_0. By comparison, the IVCT bands for symmetrical and unsymmetrical Class III complexes exhibit a weak temperature dependence due to a weak temperature dependence of H_{ab}. The present results suggest that the variations in the band-widths for the dpb-bridged complexes may be reasonably ascribed to the temperature dependence of the redox asymmetry term, *without* varying H_{ab}. For the complexes incorporating the fused bridging ligands dpq′ and dpb′, H_{ab} does appear to exhibit a weak temperature dependence which reflects the greater degree of delocalisation in these systems.

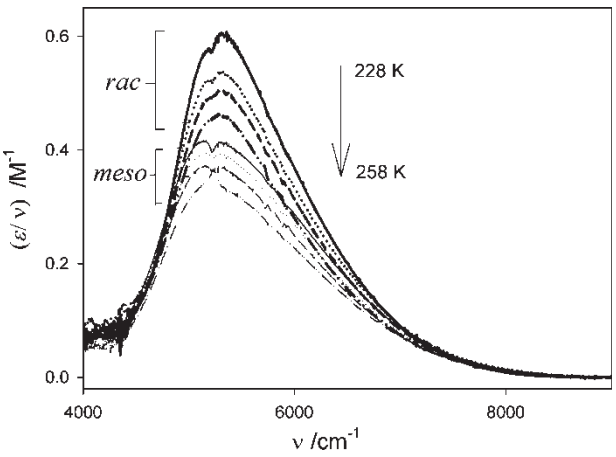

FIGURE 9 Variation of the IVCT band with temperature for the diastereoisomers of $[\{Ru(bpy)_2\}_2(\mu\text{-dpq}')]^{5+}$ in 0.02 M [(*n*-$C_4H_9)_4N$]$\{B(C_6F_5)_4\}$/*n*-butyronitrile.

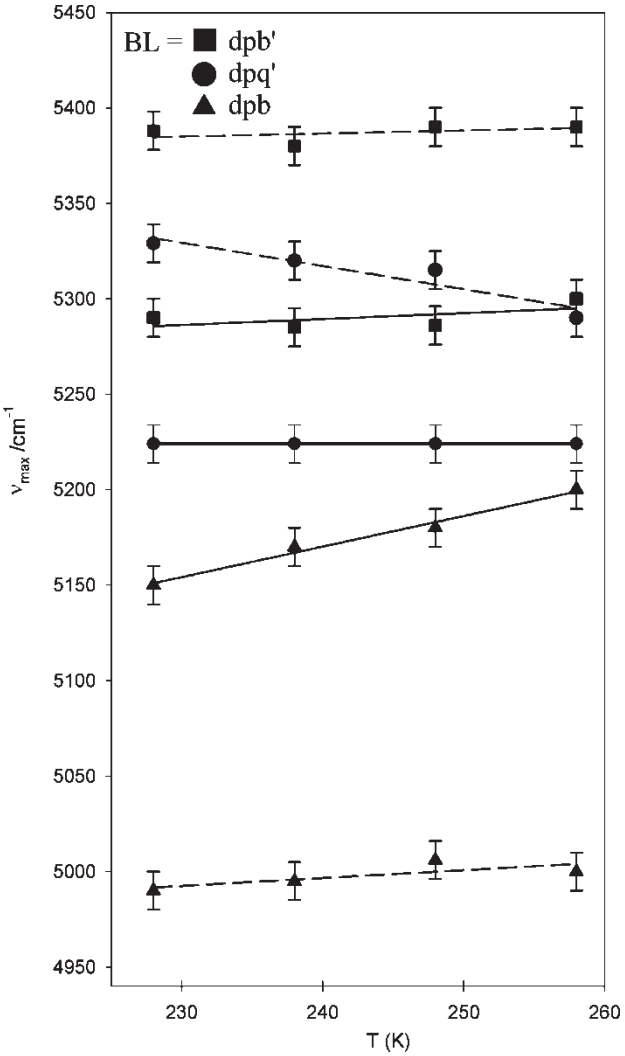

FIGURE 10 Temperature dependence of ν_{max} for the *meso* (solid line) and *rac* (dashed line) diastereoisomers of $[\{Ru(bpy)_2\}_2(\mu\text{-BL})]^{5+}$ {BL = dpb, dpb′, dpq′} in 0.02 M [(*n*-$C_4H_9)_4N$]$\{B(C_6F_5)_4\}$/*n*-butyronitrile over the temperature range −45°C (228 K) to −15°C (258 K).

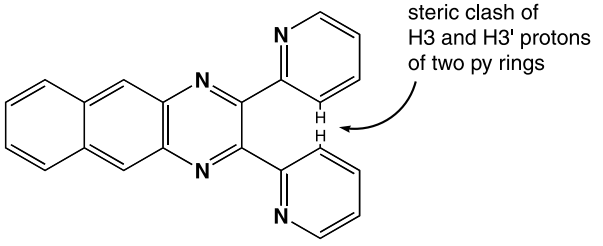

FIGURE S1 The bridging ligand 2,2-bis(2-pyridyl) benzoquinoxaline (dpb), showing the steric clash of the pyridine H3 and H3′ protons.

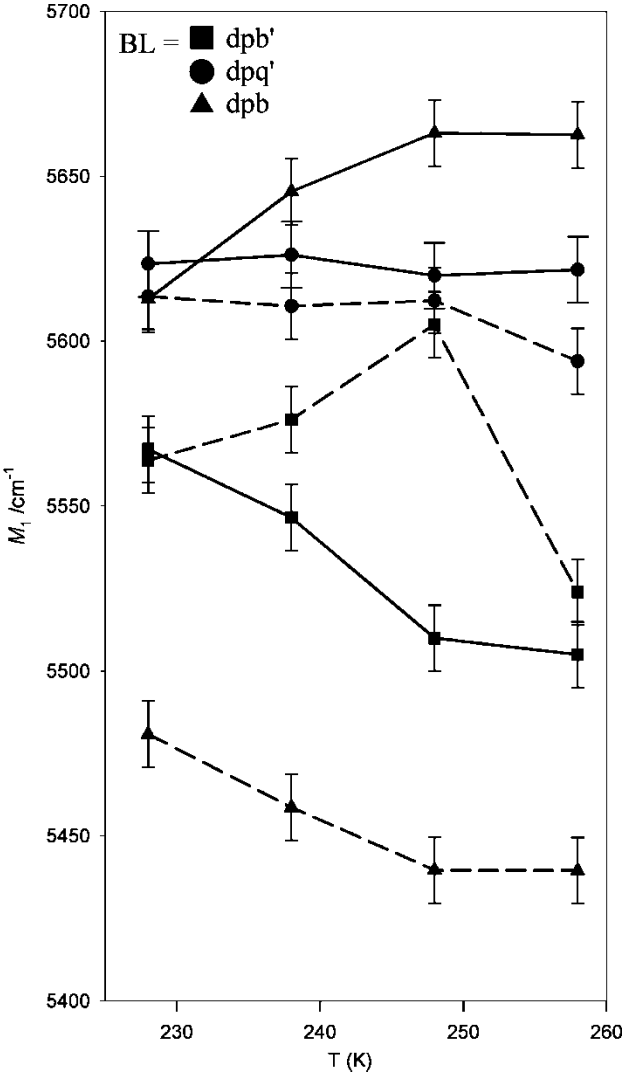

FIGURE S2 Temperature dependence of M_1 for the *meso* (solid line) and *rac* (dashed line) diastereoisomers of $[\{Ru(bpy)_2\}_2(\mu\text{-BL})]^{5+}$ {BL = dpb, dpb′, dpq′} in 0.02 M $[(n\text{-}C_4H_9)_4N]\{B(C_6F_5)_4\}$/*n*-butyronitrile over the temperature range −45°C (228 K) to −15°C (258 K).

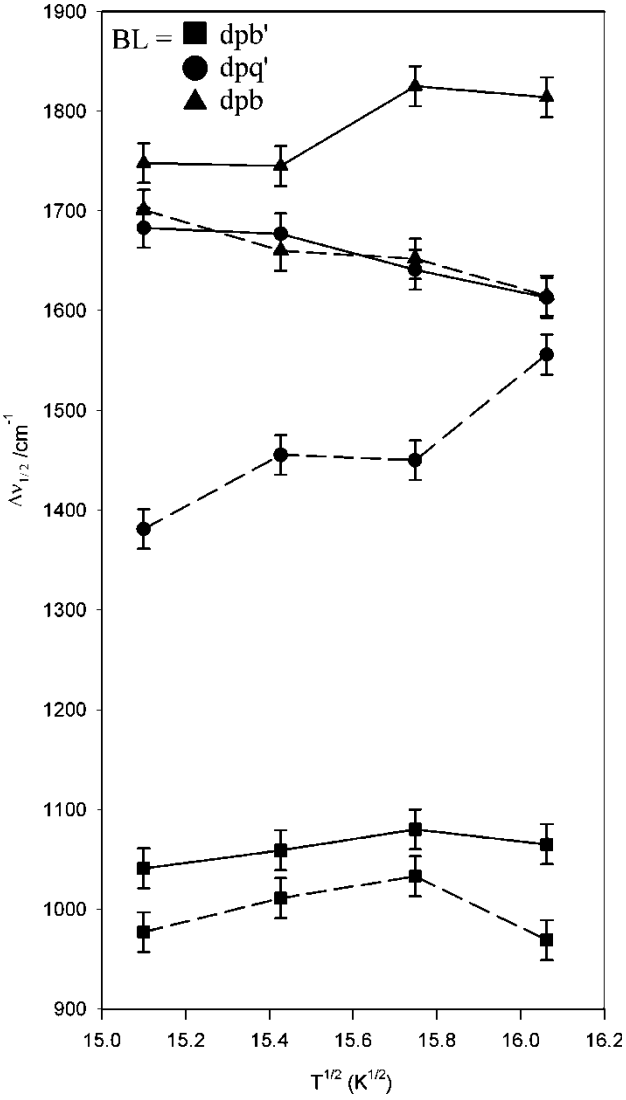

FIGURE S3 Temperature dependence of $\Delta\nu_{1/2}$ for the *meso* (solid line) and *rac* (dashed line) diastereoisomers of $[\{Ru(bpy)_2\}_2(\mu\text{-BL})]^{5+}$ {BL = dpb, dpb′, dpq′} in 0.02 M $[(n\text{-}C_4H_9)_4N]\{B(C_6F_5)_4\}$/*n*-butyronitrile over the temperature range −45°C (228 K) to −15°C (258 K).

Alternate origins for the temperature dependencies have been proposed, such as the temperature dependence of the outer sphere reorganisational energy [100]. Since the effects should be minimised by the comparison of the diastereoisomers of the same complex, and for the same diastereoisomer of different complexes, the origin of the temperature dependence of the IVCT parameters should lie in other factors.

CONCLUSIONS

The influence of stereochemical and structural factors on reorganisational energies and redox asymmetry (ΔE_0) contributions to the electron transfer barrier [expressed by Eq. (1)] have been considered, by investigation of the diastereoisomers of a series dinuclear ruthenium complexes $[\{Ru(bpy)_2\}_2(\mu\text{-BL})]^{5+}$ incorporating the bridging ligands dpb, dpb′ and dpq′.

The present study extends previous work [36,93,103] which has detailed the first observation of the effect of stereochemistry on the nature of IVCT in an extensive series of homodinuclear complexes of ruthenium. Stereochemically-directed solvent and anion interactions have been shown to be manifest in differential characteristics of the IVCT bands of the diastereoisomeric forms of the same complex.

IVCT thermochromism studies on the diastereoisomers of $[\{Ru(bpy)_2\}_2(\mu\text{-BL})]^{5+}$ in the presence of the weakly-ion pairing electrolyte $[(n\text{-}C_4H_9)_4N]\{B(C_6F_5)_4\}$ revealed that both diastereoisomers of the dpb′-bridged complex are delocalised, while the *meso* diastereoisomer of the dpq′-bridged complex is more delocalised than its *rac* analogue. For the

dpb-bridged diastereoisomers, the *rac* form is delocalised while the *meso* form exhibits a slight temperature dependence which is dependent on the identity of the counter-anion (PF_6^- or $\{B(C_6F_5)_4\}^-$). This suggests that the redox asymmetry contribution is weakly temperature dependent.

An investigation of differential stereochemically-directed anion effects on the IVCT properties of the diastereoisomeric forms of $[\{Ru(bpy)_2\}_2(\mu\text{-BL})]^{5+}$ {BL = dpb′, dpq′ and dpb} in the presence of relatively strong (PF_6^-) and weak ($\{B(C_6F_5)_4\}^-$) ion-pairing electrolytes [57] reveal the unpredictable nature of ion-pairing effects.

The realisation that metal-metal interactions in dinuclear polypyridyl complexes can be modified by the variation of their stereochemical properties has important consequences for controlling the metal-metal interaction in higher nuclearity polymetallic assemblies. The physical consequences of such factors have implications for understanding natural processes such as photosynthesis, and for the control of electron migration in metallosupramolecular assemblies designed for artificial light-harvesting applications.

Acknowledgements

We thank the Australian Research Council for financial support.

References

[1] Marcus, R. A. *J. Chem. Phys.* **1957**, *26*, 867.
[2] Marcus, R. A. *J. Chem. Phys.* **1956**, *24*, 966.
[3] Hush, N. S. *Prog. Inorg. Chem.* **1967**, *8*, 391.
[4] Hush, N. S. *Electrochim. Acta* **1968**, *13*, 1005.
[5] Robin, M. B.; Day, P. *Adv. Inorg. Chem. Radiochem.* **1967**, *10*, 247.
[6] Demadis, K. D.; Hartshorn, C. M.; Meyer, T. J. *Chem. Rev.* **2001**, *101*, 2655.
[7] Creutz, C.; Newton, M. D.; Sutin, N. *J. Photochem.* **1994**, *82*, 47.
[8] Cave, R. J.; Newton, M. D. *Chem. Phys. Lett.* **1996**, *249*, 15.
[9] Hush, N. S. *Coord. Chem. Rev.* **1985**, *64*, 135.
[10] Creutz, C. *Prog. Inorg. Chem.* **1983**, *30*, 1.
[11] Crutchley, R. J. *Adv. Inorg. Chem.* **1994**, *41*, 273.
[12] Kalyanasundaram, K.; Nazeeruddin, M. K. *Inorg. Chim. Acta* **1994**, *226*, 213.
[13] Ward, M. D. *Chem. Soc. Rev.* **1995**, *24*, 121.
[14] Barbara, P. F.; Meyer, T. J.; Ratner, M. A. *J. Phys. Chem.* **1996**, *100*, 13148.
[15] Launay, J. -P. *Chem. Soc. Rev.* **2001**, *30*, 386.
[16] Kaim, W.; Klein, A.; Glöckle, M. *Acc. Chem. Res.* **2000**, *33*, 755.
[17] Chen, P.; Meyer, T. J. *Chem. Rev.* **1998**, *98*, 1439.
[18] Nelsen, S. F. *Chem. Eur. J.* **2000**, *6*, 581.
[19] Nelsen, S. F.; Trieber, II, D. A.; Ismagilov, R. F.; Teki, Y. *J. Am. Chem. Soc.* **2001**, *123*, 5684.
[20] Hupp, J. T.; Weaver, M. J. *Inorg. Chem.* **1984**, *23*, 3639.
[21] Katriel, J.; Ratner, M. A. *J. Phys. Chem.* **1989**, *93*, 5065.
[22] Drago, R. S.; Richardson, D. E.; George, J. E. *Inorg. Chem.* **1997**, *36*, 25.
[23] Barthel, E. R.; Martini, I. B.; Schwartz, B. J. *J. Phys. Chem. B* **2001**, *105*, 12230.
[24] Matyushov, D. V.; Schmid, R. *J. Phys. Chem.* **1994**, *98*, 5152.
[25] Sullivan, B. P.; Curtis, J. C.; Kober, E. M.; Meyer, T. J. *Nouv. J. Chim.* **1980**, *4*, 643.
[26] Roberts, J. A.; Hupp, J. T. *Inorg. Chem.* **1992**, *31*, 157.
[27] Blackbourn, R. L.; Hupp, J. T. *J. Phys. Chem.* **1988**, *92*, 2817.
[28] Blackbourn, R. L.; Hupp, J. T. *Inorg. Chem.* **1989**, *28*, 3786.
[29] Hupp, J. T.; Weydert *J. Inorg. Chem.* **1987**, *26*, 2657.
[30] Ennix, K. S.; McMahon, P. T.; de la Rosa, R.; Curtis, J. C. *Inorg. Chem.* **1987**, *26*, 2660.
[31] Brunschwig, B. S.; Ehrenson, S.; Sutin, N. *J. Phys. Chem.* **1986**, *90*, 3657.
[32] Hupp, J. T.; Neyhart, G. A.; Meyer, T. J.; Kober, E. M. *J. Phys. Chem.* **1992**, *96*, 10820.
[33] Hupp, J. T.; Dong, Y. H. *J. Am. Chem. Soc.* **1993**, *115*, 6428.
[34] Dong, Y.; Hupp, J. T. *Inorg. Chem.* **1992**, *31*, 3322.
[35] Catterjee, D.; Bajaj, H. C.; Das, A. *Inorg. Chim. Acta* **1994**, *224*, 189.
[36] D'Alessandro, D. M.; Kelso, L. S.; Keene, F. R. *Inorg. Chem.* **2001**, *40*, 6841.
[37] Khoshtariya, D. E.; Bajaj, H. C.; Tregloan, P. A.; van Eldik, R. *J. Phys. Chem. A* **2000**, *104*, 5535.
[38] Hammack, W. S.; Drickamer, H. G.; Lowery, M. D.; Hendrickson, D. N. *Inorg. Chem.* **1988**, *27*, 1307.
[39] Nelsen, S. F.; Ismagilov, R. F. *J. Phys. Chem. A* **1999**, *103*, 5373.
[40] Marcus, R. A. *J. Phys. Chem. B* **1998**, *102*, 10071.
[41] Pereztejeda, P.; Neto-Ponce, P.; Sánchez, F. *J. Chem. Soc., Dalton Trans.* **2001**, 1686.
[42] Lau, K. W.; Hu, A. M. H.; Yen, M. H. J.; Fung, E. Y.; Grzybicki, S.; Matamoros, R.; Curtis, J. C. *Inorg. Chim. Acta* **1994**, *226*, 137.
[43] Lewis, N. A.; Obeng, Y. S.; Purcell, W. L. *Inorg. Chem.* **1989**, *28*, 3796.
[44] Lewis, N. A.; Obeng, Y. S. *J. Am. Chem. Soc.* **1988**, *110*, 2306.
[45] D'Alessandro, D. M.; Keene, F. R. *Chem. Phys.* **2005**, in press.
[46] Creutz, C.; Chou, M. H. *Inorg. Chem.* **1987**, *26*, 2995.
[47] de la Rossa, R.; Chang, P. J.; Salaymeh, F.; Curtis, J. C. *Inorg. Chem.* **1985**, *24*, 4229.
[48] Barigelletti, F.; De Cola, L.; Balzani, V.; Hage, R.; Haasnoot, J. G.; Reedijk, J.; Vos, J. G. *Inorg. Chem.* **1991**, *30*, 641.
[49] Hage, R.; Dijkhuis, A. H. J.; Haasnoot, J. G.; Prins, R.; Reedijk, J.; Buchanan, B. E.; Vos, J. G. *Inorg. Chem.* **1988**, *27*, 2185.
[50] Hage, R.; Haasnoot, J. G.; Nieuwenhuis, H. A.; Reedijk, J.; De Ridder, D. J. A.; Vos, J. G. *J. Am. Chem. Soc.* **1990**, *112*, 9245.
[51] Hage, R. *Coord. Chem. Rev.* **1991**, *111*, 161–166.
[52] Buchanan, B. G.; Vos, J. G.; Kaneko, M.; van der Putten, W. J. M.; Kelly, J. M.; Hage, R.; de Graaff, R. A. G.; Haasnoot, J. G.; Reedijk, J. *J. Chem. Soc., Dalton Trans.* **1990**, 2425.
[53] van Diemen, J. H.; Hage, R.; Haasnoot, J. G.; Lempers, H. E. B.; Reedijk, J.; Vos, J. G.; De Cola, L.; Barigelletti, F.; Balzani, V. *Inorg. Chem.* **1992**, *31*, 3518.
[54] Al-Noaimi, M.; Yap, G. P. A.; Crutchley, R. J. *Inorg. Chem.* **2004**, *43*, 1773.
[55] Hupp, J. t.; Dong, Y. *Inorg. Chem.* **1994**, *33*, 4421.
[56] Zhang, X. L.; Yoon, D. I.; Hupp, J. T. *Inorg. Chim. Acta* **1995**, *240*, 285.
[57] LeSuer, R.; Geiger, W. E. *Angew. Chem. Int. Ed.* **2000**, *39*, 248.
[58] Chatterjee, D.; Bajaj, H. C.; Das, A. *Inorg. Chim. Acta* **1994**, *224*, 189.
[59] Zhao, X.; Burt, J. A.; Knorr, F. J.; McHale, J. L. *J. Phys. Chem. A* **2001**, *105*, 11110.
[60] Prassides, K.; Day, P. *J. Chem. Soc., Farad. Trans. 2* **1984**, *80*, 85.
[61] Chatterjee, D.; Bajaj, H. C.; Das, A. *Inorg. Chem.* **1993**, *32*, 4049.
[62] Coropceanu, V.; Lambert, C.; Nöll, G.; Brédas, J. L. *Chem. Phys. Lett.* **2003**, *373*, 153.
[63] Blackbourn, R. L.; Dong, Y.; Lyon, L. A.; Hupp, J. T. *Inorg. Chem.* **1994**, *33*, 4446.
[64] Blackbourn, R. L.; Hupp, J. T. *J. Phys. Chem.* **1990**, *94*, 1788.
[65] Duff, C. M.; Heath, G. A. *Inorg. Chem.* **1991**, *30*, 2528.
[66] D'Alessandro, D. M.; Keene, F. R. *Chem. Eur. J.* **2005**, 3679.
[67] Ohrenberg, C.; Geiger, W. E. *Inorg. Chem.* **2000**, *39*, 2948.
[68] Hill, M. G.; Lamanna, W. M.; Mann, K. R. *Inorg. Chem.* **1991**, *30*, 4687.
[69] Lowery, M. D.; Hammack, W. S.; Drickamer, H. G.; Hendrickson, D. N. *J. Am. Chem. Soc.* **1987**, *109*, 8019.
[70] Yeomans, B. D.; Kelso, L. S.; Tregloan, P. A.; Keene, F. R.; Eur *J. Inorg. Chem.* **2001**, 239.

[71] Kelso, L. S., PhD Thesis, James Cook University, **2000**.
[72] Togano, T.; Nagao, N.; Tsuchida, M.; Kumakura, H.; Hisamatsu, K.; Howell, F. S.; Mukaida, M. *Inorg. Chim. Acta* **1992**, *195*, 221.
[73] Blessing, R. H. *Acta. Cryst.* **1995**, *A51*, 33.
[74] Sheldrick, G. M., University of Göttingen, 1997.
[75] Barbour, L. J. *J. Supramol. Chem.* **2001**, *1*, 189.
[76] Flack, H. D. *Acta Cryst.* **1983**, *A39*, 876.
[77] Anderson, P. A.; Anderson, R. F.; Furue, M.; Junk, P. C.; Keene, F. R.; Patterson, B. T.; Yeomans, B. D. *Inorg. Chem.* **2000**, *39*, 2721.
[78] Jandrasics, E. Z.; Keene, F. R. *J. Chem. Soc., Dalton Trans.* **1997**, 153.
[79] Rutherford, T. J.; Van Gijte, O.; Kirsch - De Mesmaeker, A.; Keene, F. R. *Inorg. Chem.* **1997**, *36*, 4465.
[80] Fletcher, N. C.; Junk, P. C.; Reitsma, D. A.; Keene, F. R. *J. Chem. Soc., Dalton Trans.* **1998**, 133.
[81] Rutherford, T. J.; Keene, F. R. *J. Chem. Soc., Dalton Trans.* **1998**, 1155.
[82] Keene, F. R. *Chem. Soc. Rev.* **1998**, *27*, 185.
[83] Rutherford, T. J.; Keene, F. R. *Inorg. Chem.* **1997**, *36*, 3580.
[84] Bardwell, D.; Jeffery, J. C.; Joulie, L.; Ward, M. D. *J. Chem. Soc., Dalton Trans.* **1993**, 2255.
[85] Bardwell, D. A.; Horsburgh, L.; Jeffery, J. C.; Joulié, L. F.; Ward, M. D.; Webster, I.; Yellowlees, L. J. *J. Chem. Soc., Dalton Trans.* **1996**, 2527.
[86] Balzani, V.; Bardwell, D. A.; Barigelletti, F.; Cleary, F. L.; Guardigli, M.; Jeffery, J. C.; Sovrani, T.; Ward, M. D. *J. Chem. Soc., Dalton Trans* **1995**, 3601.
[87] Baitalik, S.; Flörke, U.; Nag, K. *J. Chem. Soc., Dalton Trans.* **1999**, 719.
[88] Masui, H.; Freda, A. L.; Zerner, M. C.; Lever, A. B. P. *Inorg. Chem.* **2000**, *39*, 141.
[89] Seneviratne, D. S.; Uddin, M. J.; Swayambunathan, V.; Schlegel, H. B.; Endicott, J. F. *Inorg. Chem.* **2002**, *41*, 1502.
[90] Molnar, S. M.; Neville, K. R.; Jensen, G. E.; Brewer, K. J. *Inorg. Chim. Acta* **1993**, *206*, 69.
[91] Giuffrida, G.; Campagna, S. *Coord. Chem. Rev.* **1994**, *135*, 517.
[92] Juris, A.; Barigelletti, S.; Campagna, S.; Balzani, V.; Belser, P.; von Zelewsky, A. *Coord. Chem. Rev.* **1988**, *84*, 85.
[93] D'Alessandro, D. M.; Keene, F. R. *Dalton Trans.* **2004**, 3950.
[94] Wallace, A. W.; Murphy, W. R.; Petersen, J. D. *Inorg. Chim. Acta* **1989**, *166*, 47.
[95] Pourtois, G.; Beljonne, D.; Moucheron, C.; Schumm, S.; Mesmaeker, A. K. -D.; Lazzaroni, R.; Brédas, J. -L. *J. Am. Chem. Soc.* **2004**, *126*, 683.
[96] D'Alessandro, D. M.; Dinolfo, P. H.; Davies, M. S.; Hupp, J. T.; Keene, F. R.; submitted for publication.
[97] Reimers, J. R.; Hush, N. S. *Inorg. Chem.* **1990**, *29*, 3686.
[98] Brunschwig, B. S.; Creutz, C.; Sutin, N. *Chem. Soc. Rev.* **2002**, *31*, 168.
[99] Derr, D. L.; Elliott, C. M. *J. Phys. Chem. A* **1999**, *103*, 7888–7893.
[100] Brunschwig, B. S.; Sutin, N. *Coord. Chem. Rev.* **1999**, *187*, 233.
[101] Blackbourn, R. L.; Hupp, J. T. *Chem. Phys. Lett.* **1988**, *150*, 399.
[102] Johnson, R. C.; Hupp, J. T. *J. Am. Chem. Soc.* **2001**, *123*, 2053.
[103] D'Alessandro, D. M.; Keene, F. R.; Bergman, S. D.; Kol, M. *Dalton Trans.* **2005**, 332.